December 2016

On the Mechanical Response in Boundary Resisted Motion

Maliha Maisha Rahman
University of Wisconsin-Milwaukee

ON THE MECHANICAL RESPONSE IN BOUNDARY RESISTED MOTION

by

Maliha Maisha Rahman

A Thesis Submitted in

Partial Fulfillment of the

Requirements for the Degree of

Master of Science

in Engineering

at

The University of Wisconsin-Milwaukee

December 2016

ABSTRACT

ON THE MECHANICAL RESPONSE IN BOUNDARY RESISTED MOTION

by

Maliha Maisha Rahman

The University of Wisconsin-Milwaukee, 2016
Under the Supervision of Professor Anoop Dhingra

In engineering and science literature, there seems to be a lack of consensus on a modeling framework clarifying how resistance to boundary motion affects mechanical performance. By mechanical performance, is implied the action of a force moving an object from one point to another that generates changes in position, velocity, acceleration and jerk. Apart from affecting a whole vehicle, critical power transmission components and subcomponents all rely on the mechanical responses that change due to an applied force. For example, the power needed to move an aircraft, an automobile, a ship, a submarine etc. will be reduced if resistance to their motion diminishes.

Of the three laws of friction, the first one stating friction as directly proportional to normal load is well known and almost universally proven. The second law asserting friction as independent of the area of contact has been found not to apply when rough surfaces are considered. Finally, the third law of friction proposing friction as independent of sliding velocity remains paradoxical considering that the dependence of friction on sliding velocity emerges demonstrably from the Stribeck effect and Stokes' law of aerodynamic drag. To understand the dependence of friction on sliding velocity, this thesis establishes a

deterministic framework for identifying boundary resistance effects on mechanical responses such as distance, velocity, acceleration, jerk, frequency, interacting forces, and efficiency. For this study, two cases are considered. The first case is considered to understand the effect of boundary friction and aerodynamic drag on mechanical sliding motion. In the second case, the effects of boundary friction on spring-resisted motion are explored. These two cases are further broken down into two subcases, where the effects of constant and variable applied forces are separately investigated. The theoretical modeling effort shows that in general boundary resistance like solid friction and aerodynamic drag detrimentally impacts mechanical responses including efficiency during sliding. The deterministic framework created will be important for studying, synthesizing and designing future sustainable energy-efficiency technologies while dramatically improving existing technologies.

To the greatest and kindest woman, who taught me how to be strong in hard times, My Lovely Mother, Shaleha Rahman

To the greatest man, whom I am proud to be his daughter, My Dear Father, Md Mujahidur Rahman

And

To my loving husband Md Tarik Khan, whose support gave me strength to be where I am today.

TABLE OF CONTENTS

LIST OF FIGURES

LIST OF TABLES

ACKNOWLEDGMENTS

I owe my gratitude to my God (Allah) who granted and still grants me invaluable blessings. I thank You for Your will to let me do my masters and writing my thesis. You always give me reasons to make my goals achieved.

From that belief, I have to seize the opportunity in this part to express my deepest gratitude and appreciations to my former advisor, Dr. Emmanuel Wornyoh and my present advisor, Dr. Anoop Dhingra. I have been amazingly privileged to work with a brilliant mind like Dr. Wornyoh. He funded me for first three semesters at the tribology and energy diagnostics laboratory (TEDL). He gave me the freedom to explore on my own, and at the same time the guidance to recover when my steps paused. Later, it was very kind of Dr. Dhingra to take me under his supervision without any hesitation. Thank you for your support with everything. You gave me the chance and opened the door for me to stay here and pursue my graduate study while others closed it. I will never forget your favor for the rest of my life.

I am grateful to have worked in Industrial Assessment Center (IAC) where I have been taught so much by Dr. Emmanuel Wornyoh, Dr. Benjamin Church, Dr. John Reisel and Dr. Chris Yingchun Yuan. They have been so kind and patient to teach me everything about energy efficiency analysis. Also, I extend my gratitude to my former TEDL colleagues and associates including Dr. Divyeshkumar Patel, Dr. Emmanuel O. Asante-Asamani, Robert J. Morien, and Olaniyi S. Iyiola. Many thanks to Mr. Dan Beller for assisting me in many ways while being his teaching assistant and also for helping me with the equipment for conducting my thesis experiments. I am also grateful to Ms. Betty Warras, Ms. Gerri Meloy

and Mr. David Raschke for their unwavering assistances. I again would like to thank Dr. Benjamin Church and Dr. John Reisel for serving on my thesis committee. Thank you for your valuable time, as well as the advice and encouragements you provided me during my studies here. I want to further extend my gratitude to all academic staff, colleagues, and the friends I met at UW-Milwaukee who helped variously with my research work. At the end, words cannot describe my gratitude to my mother, father, husband and mother-in-law for believing in my abilities and ambitions, and for supporting me through all my challenges and successes. I also would like to thank Nabila Rubaiya and my other friends who always been there when I needed them.

Chapter 1

Introduction, Background Review and Significance

In these early stages of the 21st Century, global concerns about greenhouse gas (GHG) emissions have reinvigorated research efforts seeking lasting green, renewable, and sustainable and energy efficient engine technologies. Growing concerns about the efficient performance of energy consuming and energy producing technologies intensify when considering energy systems that depend on non-renewable fuel resources such as petroleum and coal. Fossil fuel sources like petroleum and coal take millions of years to form. Hence, without finding lasting alternative fuel resources that replace fossil fuels, humanity's very survival may be jeopardized.

Among a plethora of theories, it seems reasonable to safeguard technologies like internal combustion engines (ICE) that have reliably powered automobiles, aircraft, and spacecraft, marine, submarine and advanced manufacturing engines. To safeguard ICE technologies it is imperative to create deterministic frameworks for minimizing and hopefully eliminating the detrimental mechanical effects that impede performance by reducing efficiency. Apart from promoting existing ICE technologies, a successful deterministic, optimal efficiency framework will bolster emerging alternate fuels and engine technologies like fuel cells, electric hybrids, solar powered vehicles etc.

1.1 Motivation for this study

The key motivation for this thesis is the desire to reduce energy loss due to friction and thereby improve equipment efficiency. There is a global push for renewable energy by governments, academia and industry [1] to reduce GHG (Greenhouse gases) by reducing carbon footprint. It is generally believed that by reducing interfacial friction and other boundary resistances that deplete energy, the amount of harmful effluents from burning fossil fuels will be minimized. But understanding frictional dissipation remains scientifically challenging. Indeed, because of its multiscale, nonlinear nature, incorporating frictional dissipation into dynamical modeling framework remains problematic [2, 3].

Tribologists study friction, lubrication, wear, and technologies for designing bearings [4-7]. In a dynamical system, the presence of friction reduces interfacial or relative motion between components and subcomponents. Thus, if inadequate lubrication persists, then power losses, wear, heat generation, noise and other undesirable effects occur. The detrimental effects posed by friction may potentially shut down plant operations and cause valuable time loss. Additionally, frictional dissipation may directly affect energy and efficiency loss and hence equipment lifetime for automobiles and manufacturing systems [8, 9].

An understanding of the mechanisms underlying how friction affects sliding or relative motion will critically facilitate the design decisions affecting sustainable,

renewable, and energy efficiency technologies. Unfortunately, reconciling the prevailing laws of friction within dynamical modeling framework has been challenging.

1.2 Drag and boundary friction effects on motion

Advancing energy efficiency technologies require operation of critical mating components such as bearings and gears at extreme speeds and loads. To deliver their needed power, energy consuming and producing devices such as pumps, compressors, expanders, and turbines feature impellers and blades are often mounted on bearings. Consequently, whether the mounted turbine blades interact with water, steam, gas, etc. at extreme speeds, aerodynamic drag or skin friction becomes significant. As the operational speeds increase, the onset of drag on impeller blades and gear teeth may severely impact the quality of power consumed or produced. In fact recent studies suggest that boundary friction and drag severely affects the efficiency of automobile engines [9].

Tribologists rarely study the running in period associated with transient boundary lubrication and most friction data are taken post running in when sliding velocity becomes constant [10, 11]. This practice aligns well with Coulomb's law of friction asserting that friction is independent of sliding velocity [7, 12]. Coulomb's law of friction is at seeming odds with real life experience, empirical, and theoretical studies. It seems natural to expect that a high interfacial friction will lead to a lowering of sliding velocity while a low friction from novel lubrication should increase interfacial sliding velocity. Additionally, to assess how friction dissipates power and hence mechanical efficiency, it is imperative to assess the running-in period where significant friction-velocity coupling predominates in agreement with the Stribeck Effect [13, 14].

Aerodynamic drag is detrimental to operating aeronautical equipment [15] and other industrial processes [16-19] and several classification of the drag coefficient are possible. For example, apart from the basic drag coefficient C_{D0}, the skin friction drag coefficient, C_{Df}, and lift-induced drag coefficient, C_{Di} are the many different classifications used generally [20]. Drag reduction techniques have led to novel energy efficient techniques [21, 22].

From a broader perspective of resisted motion, if we reconsider frictional resistance to generally include boundary friction, aerodynamic drag or skin friction, then Coulomb's law of 1789 seemingly contradicts Stokes law of drag. In Stokes' law, aerodynamic drag force or skin friction varies directly with velocity (at low speeds) or as the square of velocity (at high speeds). Advanced transportation systems including aircraft and magnetic levitation trains aim to minimize and/or completely eliminate aerodynamic drag. What happens when drag force affects the aircraft in air [23] and how does its behavior influence the kinematic properties spatiotemporally? Apart from boundary friction, recent studies suggest that drag affects the mechanical efficiency of automobile engines [9]. When considering the motion of a passenger car, in addition to the drag force, how does boundary friction affect the dynamic properties of the car? Significant studies on how drag affects the terminal motion of a body [24-28], clouds and raindrops [29], bubbles [30-34], stellar winds [35, 36] and volcanic eruptions [37] suggest that these naturally occurring phenomena most certainly affect the horizontal motion of vehicles.

1.3 Boundary friction effects on spring-loaded object motion

The importance of studying a spring mass system is widely known. The physics of the motion of a spring mass system has been studied many times starting from introductory physics classes of high school, college, and advanced research settings. In most usual spring mass systems, a sinusoidal applied force is assumed. In this thesis, the motion of a cart that encounters resisting forces of viscous drag and boundary friction are studied. Additionally, the motion of a cart with two mechanical resisting forces, frictional force and spring was studied. The purpose of the stated studies was to understand how mechanical effects like velocity, acceleration, jerk and frequency occur spatiotemporally for two cases of an applied force:

a. A constant applied force.
b. An exponentially decreasing applied force.

We consider both cases of applied forces to be in presence of mechanical boundary resistance. By interrogating the essence of boundary resistance on motion, we reassess Coulomb's law of friction asserting that friction force is independent of the sliding velocity. Apart from contradicting real life experiences, several empirical and theoretical studies suggest that there is a significant friction-velocity interrelationship during relative motion [7, 38-41]. A better understanding of the effects of boundary fiction on the sliding velocity will help improve ways to lower the friction [42-46]. Ultimately, fundamentally understanding friction-velocity coupling will be instructive for synthesizing mechanisms for reliable artificial knee and hip joint technologies [47-50], understanding scientific and

industrial problems associated with stick slip and running-in phenomena [10, 41], molecular and atomic scale friction phenomena [44, 45, 51, 52].

1.4 Role of tribology in understanding the resistance to motion

Tribology is the study of the principles and applications of friction, lubrication and wears and includes multidisciplinary areas like mechanical engineering and materials science. The importance of tribology in the field of energy is undeniable [4-7, 53]. The loss of efficiency in energy producing devices and energy consuming devices is mostly caused by friction and wear. Mechanical wear includes adhesive, fatigue, abrasion, erosion and corrosion, which reportedly cause expensive industrial losses. For example, industrial annual losses in USA due to wear and friction amounting 1-2% of GDP has been reported [54]. To reduce friction and wear requires novel lubrication technologies. Reliable science-based technologies bolstered by deterministic modeling with minimal sacrificial assumptions and adequately matching realistic experiments will be pivotal [2, 3, 55]. The growing importance of tribology at micro and nano-scales is generating renewed interests in recent times and valuable, deterministic science-based insights will transform the study of how frictional resistance at submicron and nano scales controls interfacial macroscale motion.

1.5 Friction

Friction is the mechanical interfacial force opposing the force applied to move an object. Friction acts in the opposite direction to motion and examples include but not limited to:

1. Boundary friction at solid-solid interfaces
2. Fluid friction from viscous shearing between different fluid streams
3. Solid-fluid interfacial friction arising from lubricated contacts
4. Skin friction from aerodynamic drag during fluid-solid surface interactions

Solid-solid and/or solid-fluid-solid frictional interactions may be static or kinetic friction depending on the dynamics of sliding interfaces. Static friction is the friction, which is necessary to overcome the initial resistance keeping an object from sliding while kinetic friction is the friction persisting wile an object is still moving. Static friction is always greater than kinetic friction [4, 5, 7, 56].

The prevailing three empirical laws of friction [57] are:

1. Amonton's first law: The force of friction is directly proportional to the applied load
2. Amonton's second law: The force of friction is independent of the apparent area of contact
3. Coulomb's law of friction: Kinetic friction is independent of the sliding velocity

Amonton's first law is well known and almost universally proven. Amonton's second law ($F_f \neq f$ (apparent area of contact)) also has been proven when rough surfaces are considered. But, the 3rd law ($F_f \neq f$ (sliding velocity)) is contradicted by Stribeck effect and Stokes' law of aerodynamic drag. For example, viscous friction which is also known as aerodynamic drag can be expressed as $F_D = \rho C_D A v^2 / 2$ where F_D is the drag force, ρ is the fluid density, C_D is the dimensionless drag coefficient, A is the moving object's cross-sectional or reference area, and v is the flow velocity relative to the object. To understand if Coulomb's law is universal, it is will be instructive to reconcile it with Stokes' law of drag

within the context of a dynamical system moving in the presence of boundary resistance other than drag.

1.6 Research objectives

The objectives of this thesis are as follows:

1. Generalize boundary resistance to motion to include all mechanical effects impeding motion, for example, drag, inertial weight and solid-solid boundary friction.
2. Create a deterministic framework for examining interfacial friction effect on sliding motion. Assuming a known applied force, a prototypical dynamical system is constructed to determine how friction directly affects mechanical efficiency.
3. Conduct basic experiments to test the theoretical results establishing deterministic interfacial friction.
4. Suggest model refinements based on the matchup between experiments and modeling.

Chapter 2

Theoretical Modeling of Boundary Resisted Motion

Boundary resistance will generally impede mechanical responses of all kinds. Mechanical responses are kinematic and dynamic effects that may be independent or interdependent resulting from forces causing an object's motion. Generally, a boundary resistance may comprise solid-solid, solid-fluid or solid-solid-fluid, solid-fluid-solid, solid-solid-solid mechanical impedance to motion. In other words, material media that oppose an object's motion are usually transmitted at its boundary. For example:

a. Solid- solid resistances may be boundary friction and spring.
b. Solid-fluid-solid resistances may be boundary friction, drag and spring.
c. Solid-solid-solid boundary friction may occur on an interface lubricated by a solid lubricant film, significant viscous damping and/or spring restraint.

2.1 Modeling Objective

The main modeling objective was to create a modeling framework for deterministically quantifying mechanical responses occurring in the presence of boundary resistance. The modeling was facilitated by dividing the mechanical responses into two types: primary and secondary responses.

1. The primary responses in the presence of boundary resistance are
    a. Distance traveled
    b. Velocity
    c. Acceleration
    d. Jerk

e. Interacting applied, resisting, and net forces.

2. The secondary responses in the presence of boundary resistance include mechanical efficiency, total energy and total energy transfer rate.

The modeling objectives were pursued by constructing two prototypical cases.

Case Study-1:

We examine the effect of drag and solid boundary friction on the motion of a sliding object.

Furthermore, this prototypical example is divided into two subcases

Subcase 1A: Here, the applied force was constant.

Subcase 1B: An exponentially decreasing applied force was used.

Case Study-2:

We examine the effects of boundary friction on a spring-loaded sliding object.

Subcase 2A: A constant applied force is used.

Subcase 2B: An exponentially decreasing applied force is used.

2.2 Methodology of theoretical modeling

The following assumptions were used to construct the theoretical models:

1. An applied force is already known which is:
   a. Constant
   b. Exponentially decreasing
2. Boundary friction is known which is:
   a. Drag force
   b. Interfacial wall friction
3. Spring force is considered generally as a mechanical restraint.
4. The nominal contacting surfaces are smooth.

5. The resultant or net force moving a given object acts at the center of mass.
6. A given object encountering boundary resistance begins from rest.

2.3 Case Study-1: Effects of boundary friction on drag-resisted horizontal motion

To generalize frictional resistance capturing the dissipation caused by boundary friction, aerodynamic drag, hydrodynamic drag, viscous drag or skin friction, it is imperative to reconcile Coulomb's law of friction, with Stokes' law of drag. On one hand, Stokes' law of drag underpins terminal motion and has been proven fundamentally in numerous theoretical and experimental studies [15, 18, 21, 22, 30, 31, 33-35, 37, 58-62]. Coulomb's law of friction suggests that friction is independent of sliding velocity and seems at odds with Stokes' law of drag if frictional resistance is generalized to accommodate viscous drag. As research continues to advance in fluid structure interactions, it seems that fundamental insights may be gleaned if boundary friction and drag were properly aligned. For example, a turbine impeller or a propeller system rotating at extreme speeds in a fluidic medium such as air or combustion gaseous products may encounter aerodynamic drag. Meanwhile, the bearing on which the propeller or turbine impeller is attached will experience boundary friction. Both sources of resistance are critical to the turbine performance and must be considered in evaluating the mechanical efficiency. Another example involves automobiles that must overcome boundary friction within the internal combustion engines that powers them, and the wheel-pavement or wheel-bearing boundary friction as well as the aerodynamic drag (see schematic in Fig. 2.1).

The objective of **Case Study-1** is to examine how boundary friction and drag may affect terminal motion. It is also of scientific and intellectual significance to determine whether the onset of terminal motion depends on the type of applied forces acting. For example does terminal motion occur regardless of whether a constant or a variable force is applied? Using the schematic in Fig. 2.1, we analyze the horizontal terminal motion (HTM) of a wheeled object traveling horizontally against a constant friction surface. The boundary friction force F_{Bf} represents the equivalent combined effect of the interfacial boundary friction force at the wheel pavement F_{fwp} and the wheel bearing F_{fwb}. The block of mass m carries a load F_n so that according to Amonton's law of friction the boundary friction force becomes $F_{Bf} = \mu F_n$ where μ is the constant friction coefficient at the moving block stationary block interface.

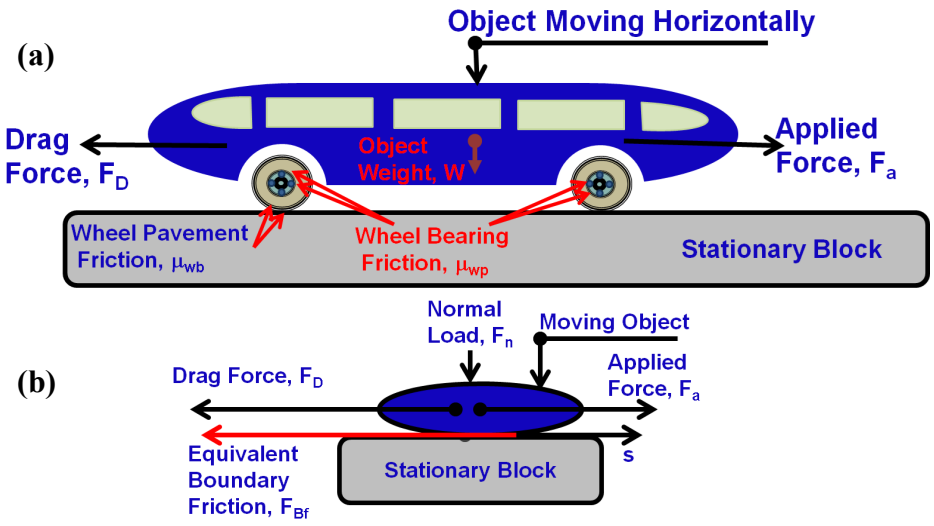

Figure 2.1: Schematic of an object executing a horizontal terminal motion (HTM)

Case Study 1 is broken into two subcases, which are:

a. Subcase 1A: A constant applied force opposed by aerodynamic drag and boundary friction

b. Subcase 1B: An exponentially decreasing force opposed by drag and boundary friction

2.3.1 Subcase 1A: Constant applied force with drag and boundary friction

Applying Newton's 2nd law of motion $F_a - F_D - F_{Bf} = F_{net} = ma$. Since we only considered an isodynamic applied force F_a, we found that only a constant boundary friction force F_{Bf} applies in this case. Otherwise, the inclusion of velocity-dependent friction effects produces non-physical results showing that the assumption of an isodynamic force breaks down. From Amonton's law of friction, we know $F_{Bf} = \mu F_n$ where μ =interfacial friction coefficient and F_n = normal load carried by sliding block. So the equation of motion becomes:

$$\frac{dv}{dt} = \frac{d^2s}{dt^2} = \frac{F_a - \mu F_n}{m} - \frac{1}{2m}\rho C_D A v^2 \qquad (2.1)$$

Terminal velocity occurs when the object's velocity is constant or its acceleration is zero. In this case, Eq. 2.1 shows that horizontal terminal velocity becomes:

$$v_T = \sqrt{\frac{2(F_a - \mu F_n)}{\rho C_D A}} \qquad (2.2)$$

As Eq. 2.2 appears, the horizontal terminal velocity is inversely proportional to the square root of density, drag coefficient, cross sectional area and directly proportional to the square root of the isodynamic force.

2.3.1.1 Spatiotemporal mechanical behavior in horizontal terminal motion:

To find how the kinetic and dynamic (i.e. the mechanical) properties of the sliding block evolves spatiotemporally, we reconsider Eq. 2.1. First of all Eq. 2.1 suggests the rate at which the block's acceleration changes with time, which is the jerk *J*, is:

$$J = \frac{da}{dt} = \frac{d^2v}{dt^2} = \frac{d^3s}{dt^3} = -\rho C_D A \frac{ds}{dt}\frac{d^2s}{dt^2} \tag{2.3}$$

Although we are interested in the block's jerk, Eq. 2.3 reveals that we need to find the velocity *v*, in order to quantify the jerk. So solving Eq. 2.1 using standard methods, we find velocity as given in Eq. 2.4.

$$v = \frac{ds}{dt} = \left(\sqrt{\varepsilon_{Bf}} \tanh\left[\frac{\alpha\sqrt{\varepsilon_{Bf}}}{2} t \right] \right) \tag{2.4}$$

Using the velocity expression, the acceleration is obtained in Eq. 2.5.

$$a = \frac{d^2s}{dt^2} = \frac{F_{a_{Bf}}}{m} - \frac{\alpha}{2}\left(\sqrt{\varepsilon_{Bf}} \tanh\left[\frac{\alpha\sqrt{\varepsilon_{Bf}}}{2} t \right] \right)^2 \tag{2.5}$$

where $\alpha = \rho C_D A / m$ and $F_{a_{Bf}} = F_a - \mu F_n$, $\varepsilon_{Bf} = 2F_{aBf} / (\alpha m)$. After applying the initial condition u_0 =0 at t=0, Eq. 2.4 can immediately be solved through direct integration to give:

$$s = \frac{2}{\alpha} \ln\left\{ \cosh\left[\frac{\alpha\sqrt{\varepsilon_{Bf}}}{2} t \right] \right\} + s_0 \tag{2.6}$$

The distance-time expression in Eq. 2.6 when inverted yields the time-distance correlation in Eq. 2.7.

$$t = \frac{2\cosh^{-1}\left[e^{\alpha(s-s_0)/2}\right]}{\alpha\sqrt{\varepsilon_{Bf}}} \tag{2.7}$$

Having obtained distance, time, velocity and acceleration, we find the instantaneous jerk as in Eq. 2.8.

$$J = -\rho C_D A\left(\sqrt{\varepsilon_{Bf}}\tanh\left[\frac{\alpha\sqrt{\varepsilon_{Bf}}}{2}t\right]\right)\left(\frac{F_{Bf}}{m} - \frac{\alpha}{2}\left(\sqrt{\varepsilon_{Bf}}\tanh\left[\frac{\alpha\sqrt{\varepsilon_{Bf}}}{2}t\right]\right)^2\right) \tag{2.8}$$

Having determined the primary kinematic responses of distance, velocity, acceleration, and jerk, we then quantify the secondary mechanical response of mechanical efficiency. Here, we want to define mechanical efficiency as the amount of useful power that is obtainable even as the object moves against the resisting force such as drag and/or boundary lubrication.

In the prototypical examples of both cases considered, we quantify how mechanical efficiency varies spatiotemporally. And, since our applied force is isodynamic, we find that if we put in the work done by this isodynamic force in moving an object through a distance s: $W_a = F_a.s$, then for power transferred isodynamically, we get, $\dot{W}_a = F_a.v$.

Defining mechanical efficiency by:

$$\eta_m = \frac{\dot{W}_{net}}{\dot{W}_a} = \frac{\text{net power transferred}}{\text{power transferred by isodynamic force}}$$

then, from the equation of motion in Eq. 2.1, we find that even though the object is moving against friction, it does so with an effective net force resulting in a net power transferred. Thus:

$$\eta_m = \frac{\dot{W}_{net}}{\dot{W}_a} = \frac{\dot{W}_a - \dot{W}_f}{\dot{W}_a} = 1 - \frac{\dot{W}_f}{\dot{W}_a} \tag{2.9}$$

To implement Eq. 2.9 for the two resistance cases, we notice that we are dealing with boundary friction and drag. For the case involving drag and boundary friction, $W_f = W_{Bf} + W_D = (F_{Bf} + F_D) \cdot s$ so that the power expended against boundary friction and drag becomes: $\dot{W}_f = \dot{W}_{Bf} + \dot{W}_D = F_{Bf} \cdot \dot{s} + \dot{F}_D \cdot s + F_D \cdot \dot{s}$. Recalling that $F_{Bf} = \mu F_n$ and $F_D = \rho A C_D v^2 / 2 = \rho A C_D \dot{s}^2 / 2$, then $\dot{W}_D = \rho A C_D s \dot{s} \ddot{s} + \rho A C_D \dot{s}^3 / 2$ and $\dot{W}_{Bf} = F_{a_{Bf}} \cdot \dot{s}$. Substituting into Eq. 2.9, we get:

$$\eta_m = 1 - \frac{\rho A C_D}{F_{a_{Bf}}} \left(\frac{2}{\alpha} \ln \left\{ \cosh \left[\frac{\alpha \sqrt{\varepsilon_{Bf}}}{2} t \right] \right\} + s_0 \right) \left(\frac{F_{a_{Bf}}}{m} - \frac{\alpha}{2} \left(\sqrt{\varepsilon_{Bf}} \tanh \left[\frac{\alpha \sqrt{\varepsilon_{Bf}}}{2} t \right] \right)^2 \right) - \frac{\rho A C_D}{2 F_{a_{Bf}}} \left(\sqrt{\varepsilon_{Bf}} \tanh \left[\frac{\alpha \sqrt{\varepsilon_{Bf}}}{2} t \right] \right)^2 \tag{2.10}$$

Clearly, Eq. 2.10 captures how drag reduces the mechanical power coming from the applied force $F_{a_{Bf}}$. As motion tends towards terminal in which case velocity approaches terminal value v_T as acceleration vanishes, η_m tends to a terminal value η_{mT} given in Eq. 2.11.

$$\eta_{mT} = 1 - \frac{\rho A C_D \dot{s}_T^{\,2}}{2 F_{a_{Bf}}} \tag{2.11}$$

We can quantify the interacting forces using Eq. 2.1.

$$F_{a_{Bf}} - F_D = m\frac{d^2s}{dt^2}$$
$$F_{net} = F_{a_{Bf}} - F_D \tag{2.12}$$

Integrating Eq. 2.11 we obtain the rate of change of total mechanical energy which for horizontal motion is the rate of change of kinetic energy as given in Eq. 2.13.

$$\dot{E}_T = \left[F_{a_{Bf}} \left(\sqrt{\varepsilon_{Bf}} \tanh\left[\frac{\alpha\sqrt{\varepsilon_{Bf}}}{2} t \right] \right) - \frac{1}{2}\rho C_D A \left(\sqrt{\varepsilon_{Bf}} \tanh\left[\frac{\alpha\sqrt{\varepsilon_{Bf}}}{2} t \right] \right)^3 \right] \tag{2.13}$$

2.3.1.2 Modeling input parameters

To interrogate the modeling results obtained, the input parameters given in Table 1 were used.

Table 2.1: Input parameters for effects of drag and boundary motion on horizontal sliding motion

Object mass	m	5 kg
Radius of the object	r	0.5 m
Density of Air	ρ	1.2754 kg/m^3
Initial velocity	u_0	0 m/s
Initial sliding distance	s_0	10^{-3} m
Initial Acceleration	a_0	9.81 m/s^2
Applied Force	F_a	30 N
Normal Force	F_n	20 N
Coefficient of Drag	C_D	0.015
Coefficient of friction	μ	[0.05, 0.15, 0.35]

2.3.1.3 Results

The illustrative plots displaying mechanical attributes of the object in the presence of boundary motion were obtained by plotting the analytical results using Matlab™ software. The instantaneous mechanical responses are shown in Figs. 2.2a to 2.2e.

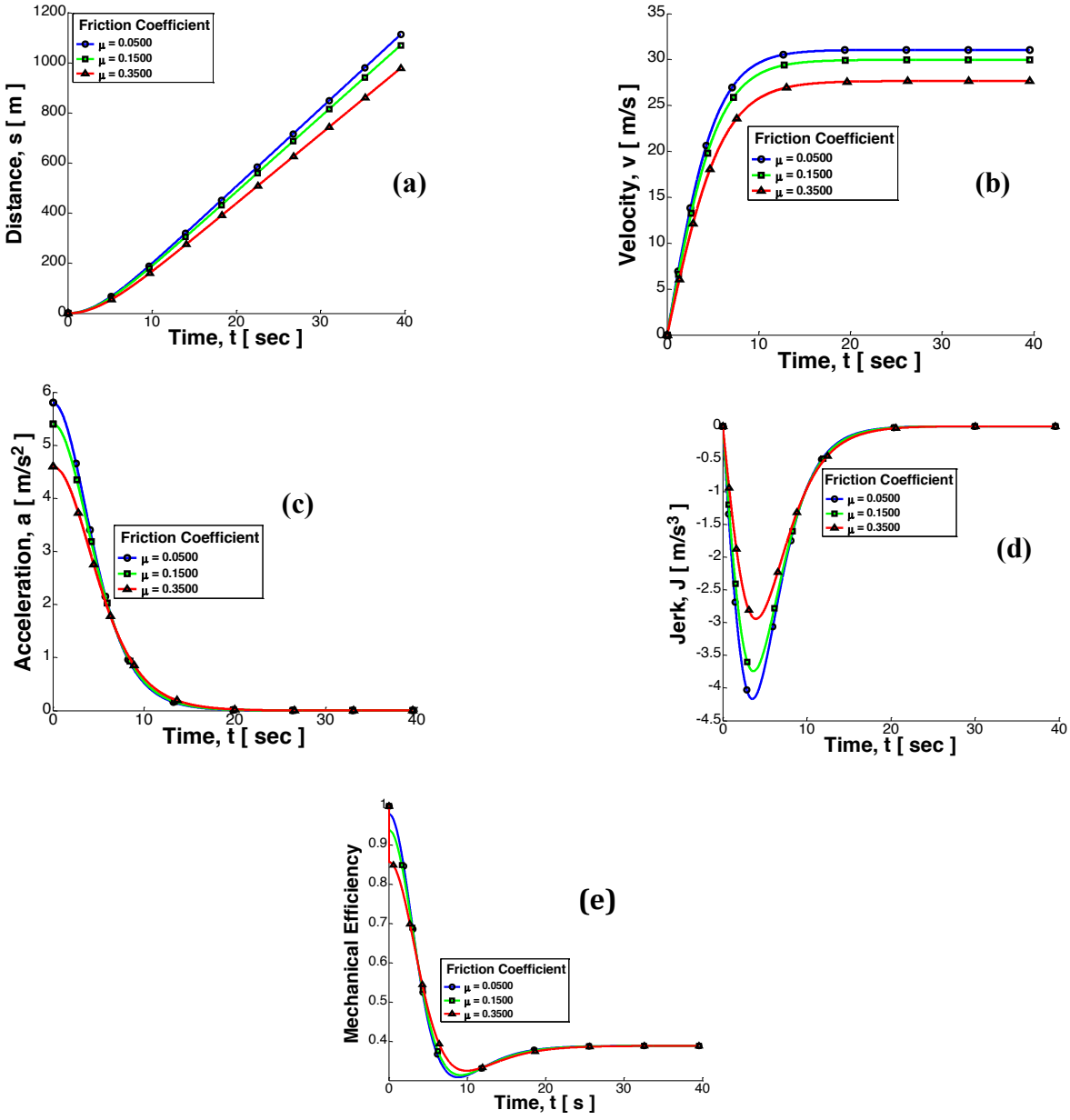

Figure 2.2: Effects of boundary friction on sliding objects when applied force is constant: (a) Distance, (b) Velocity, (c) Acceleration, (d) Jerk, (e) Mechanical efficiency

2.3.2 Subcase 1B: Exponentially decreasing force with drag and boundary friction

To test different applied forces in the presence of boundary resistance, instead of the constant or isodynamic applied force in subcase 1A, an exponentially decreasing force $F_a = F_0 e^{-s/L}$ is considered in Eq. 2.14.

$$\frac{d^2s}{dt^2} = \frac{F_0}{m} e^{-\frac{s}{L}} - \frac{1}{2m}\rho C_D A v^2 - \mu_d \frac{F_n}{m} \tag{2.14}$$

Unlike the equation of motion given in Eq. 2.1, Eq. 2.14 is problematic to solve analytically for a closed form distance-time relation needed for extracting other mechanical responses. Therefore, by applying numerical methods an approximate solution based on Newton's method is obtained in Eq. 2.15. The implementation of Newton's method to a discretized form of Eq. 2.14 leads to a general solution in Eq. 2.15.

$$X_{n+1} = X_n - [F'(X_n)]^{-1} F(X_n) \tag{2.15}$$

Where, $F(X_{n+1}) = \begin{bmatrix} f_1(X_{n+1}) & f_2(X_{n+1}) \end{bmatrix}^T$, and

$$F(X_{n+1}) = \begin{bmatrix} f_1(X_{n+1}) \\ f_2(X_{n+1}) \end{bmatrix} = \begin{bmatrix} s_{n+1} - s_n - \Delta t v_{n+1} \\ v_{n+1} - v_n - \Delta t \left(\frac{F_0}{m} e^{-\frac{s}{L}} - \frac{1}{2m}\rho C_D A v^2 - \mu_d \frac{F_n}{m} \right) \end{bmatrix}$$

and $F'(X_{n+1})$ is the Jacobian of the nonlinear residual given as:

$$F'(X_{n+1}) = \begin{bmatrix} \frac{\partial f_1}{\partial s} & \frac{\partial f_1}{\partial v} \\ \frac{\partial f_2}{\partial s} & \frac{\partial f_2}{\partial v} \end{bmatrix} = \begin{bmatrix} 1 & -\Delta t \\ A & B \end{bmatrix} \tag{2.16}$$

with $A = \Delta t F_0 e^{-s/L} / (mL)$ and $B = 1 + \Delta t \rho C_D A v / m$. By solving eq. 2.15 iteratively with the help of a Matlab™ -based Newton solver, the instantaneous mechanical responses are illustrated in Fig. 2.3

2.3.2.1 Modeling input parameters

For illustrative plots using modeling results, the input parameters chosen depend on our experiments. The input parameters are given in Table 2.2.

Table 2.2: Modeling parameters for exponentially decreasing force with drag and boundary friction

Final Time	T	4 seconds
Object mass	m	1 kg
Applied Force	F_0	.95 N
Normal Force	F_n	9.8 N
Air Density	ρ	1.225 kg/m^3
Drag Coefficient	C_D	1.2
Initial velocity	u_0	0.001 m/s
Initial sliding distance	s_0	0.001 m
Area	A	.095 m *.035 m
Friction Coefficients	μ	[.03; .04; .06; .07]
Length	L	1 m

2.3.2.2 Results

Using Matlab™ software the plots of the instantaneous kinematic properties are illustrated in Figs. 2.3a to 2.3e.

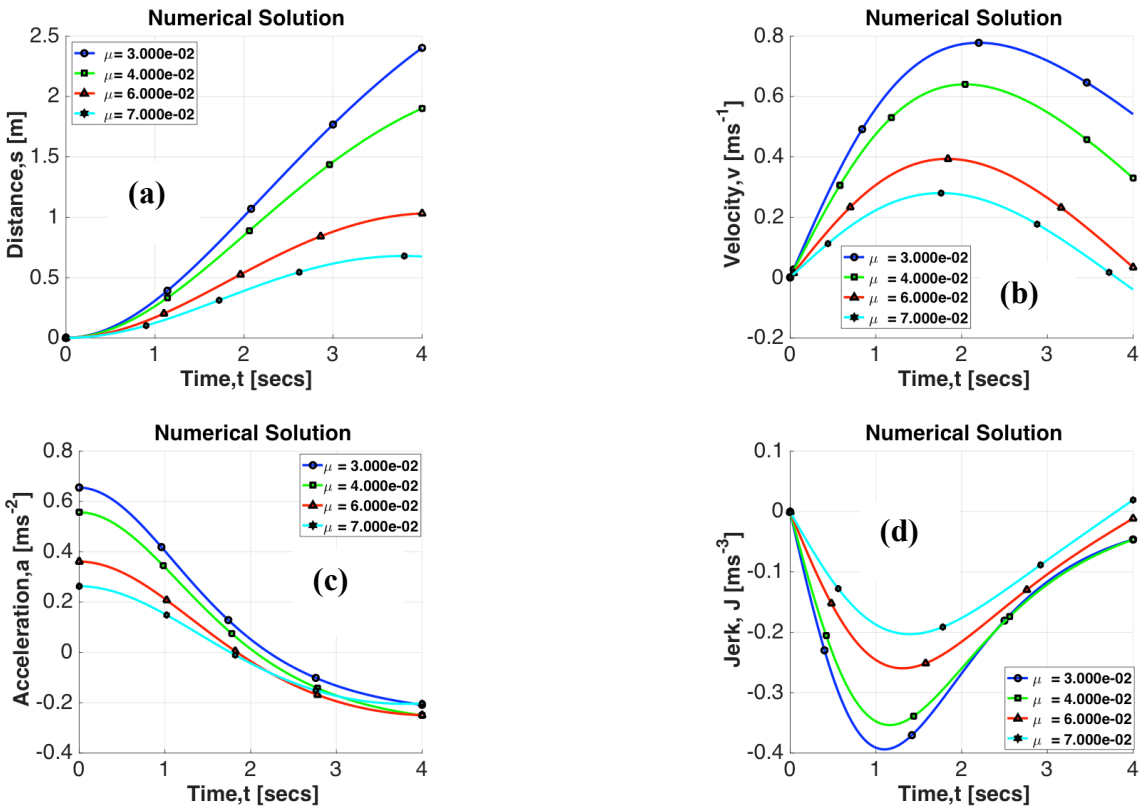

Figure 2.3: Effects of boundary friction on sliding objects when applied force exponentially decreases: (a) Sliding Distance, (b) Sliding Velocity, (c) Sliding Acceleration, (d) Sliding Jerk

2.3.3 Discussion of results

From the graphs, we can note down the following points:

1. We considered three different friction coefficients. As can be seen from Figs. 2.2a and 2.3a, for the lowest friction coefficient, the highest distance is covered.

2. Figures 2.2b and 2.3b depict that velocity is also affected by friction coefficient. The lower the friction coefficient, the higher the velocity. And the higher the friction coefficient, the lower the velocity.
3. Acceleration and jerk are also adversely affected by friction coefficients as can be seen from Figs. 2.2c, 2.2d, 2.3c and 2.3d. Under a constant applied force, acceleration is almost constant. But with a variable force, acceleration starts from a positive value and reduces to a negative value. Similarly with a constant applied force, jerk is almost close to zero but for variable force, jerk starts from zero, lowers down to a negative value then comes back up to zero again.
4. We only plotted mechanical efficiency under constant applied force i.e. in Fig. 2.2e. We can see how mechanical efficiency is directly affected by the different coefficients of friction. Mechanical efficiency increases with decreasing friction force.
5. For a constant applied force, a heavier mass of 5 kg is observed and that is why the duration of sliding is more. For an exponentially decaying force, the duration of sliding is less because the mass of the object is only 1 kg.

2.4 Case Study 2: Influence of boundary friction on a spring loaded sliding object

A spring loaded mass is a ubiquitous modeling prototype for examining mechanical responses in dynamical system of relevance to automobile engines [63-65], controls and vibrations theory [14, 66] and other specialty science areas involving atoms and subatomic

particles etc. [44, 67]. In building friction-measuring equipment such as a tribometer and an atomic force microscope (AFM), boundary friction affecting a spring-loaded sliding critical element is significant [41, 68]. In this section we focus on a sliding spring-loaded block opposed by boundary friction. We consider two subcases as done in **Case Study 1.** In both subcases the boundary friction is a constant interfacial friction force and a spring force. This prototypical example is useful for tribology test equipment, control devices or systems, cam follower etc. The sub-cases are-

a. Subcase 2A: A constant applied force opposed by a constant boundary friction.
b. Subcase 2B: An exponentially decreasing applied force opposed by a constant boundary friction.

2.4.1 Subcase 2A: A constant applied force opposed by a constant boundary friction force.

Here we examine spring-mass sliding behavior in the presence of boundary friction. From Newton's second law of motion we get $F_{net} = ma$. If we consider resisting forces as the spring ($F_{sp} = ks$) and boundary friction ($F_{Bf} = \mu F_n$) forces, then we have the desired equation of motion in Eq. 2.17.

$$\frac{d^2s}{dt^2} = \frac{F_a}{m} - \frac{k}{m}s - \frac{\mu F_n}{m} \tag{2.17}$$

Using standard methods, Eq. 2.17 is solved to obtain the instantaneous distance *s*, velocity *v*, acceleration *a* and jerk *J*. Specifically, by integrating Eq. 2.17, we get distance as in Eq. 2.18 whose subsequent differentiations yield *v*, *a*, and *J* in Eqs. 2.19, 2.20, and 2.21 respectively.

$$s = C_1 \cos(\sqrt{k/mt}) + C_2 \sin(\sqrt{k/mt}) + (F_a - \mu F_n)/k \tag{2.18}$$

$$v = -\sqrt{k/m} C_1 \sin(\sqrt{k/mt}) + \sqrt{k/m} C_2 \cos(\sqrt{k/mt}) \tag{2.19}$$

In the quantified kinematic results, the integration constants are $C_1 = (F_a - \mu F_n)/k$ and $C_2 = u_0 / \sqrt{k/m}$.

$$a = F_a/m - k\left(C_1 \cos(\sqrt{k/mt}) + C_2 \sin(\sqrt{k/mt})\right)/m + (F_a - \mu F_n)/k - \mu F_n/m \tag{2.20}$$

$$J = k\left(\sqrt{k/m} C_1 \sin(\sqrt{k/mt}) - \sqrt{k/m} C_2 \cos(\sqrt{k/mt})\right)/m \tag{2.21}$$

2.4.1.1 Modeling input parameters

To test quantified modeling results, the input parameters in Table 2.3 were used.

Table 2.3: Modeling parameters for constant applied force with boundary friction on a spring loaded sliding objects

Final Time	T	1 second
Object mass	m	1 kg
Constant Applied Force	F_0	9.3 N
Normal Force	F_n	9.8 N
Initial velocity	u_0	0.001 m/s
Initial sliding distance	s_0	0 m
Friction Coefficients	μ	[0.252;0.337; 0.4]
Spring Constant	k	116.25 m

2.4.1.2 Results

The quantified theoretical results are illustrated graphically in Figs. 2.4a to 2.4d and were obtained using Matlab™ software.

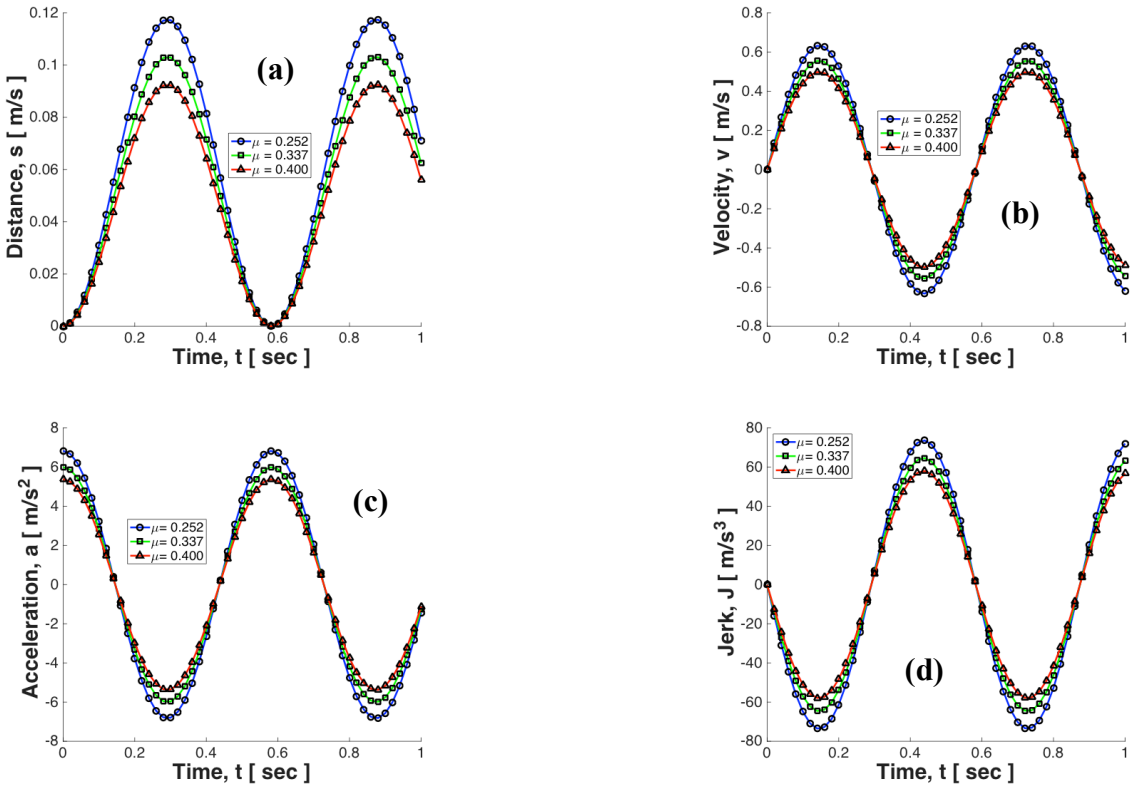

Figure 2.4: Effects of boundary friction on spring-loaded sliding objects when applied force is constant: (a) Sliding Distance, (b) Sliding Velocity, (c) Sliding Acceleration, (d) Sliding Jerk

2.4.2 Subcase 2B: An exponentially decreasing applied force opposed by a boundary friction force

To determine the effects of friction on the kinematic properties of a horizontal powered block under constant force and a spring, we had to deduce distance from acceleration. The

numerical solution was not effortless but with a variable force, it is a different scenario as we have a challenging nonlinear, nonhomogenous ordinary differential equation (ode). Using an applied force $F_a = F_0 e^{-s/L}$ gives the desired equation of motion in Eq. 2.22.

$$\frac{d^2 s}{dt^2} = \frac{F_0}{m} e^{-\frac{s}{L}} - \frac{k}{m} s - \mu_d \frac{W_n}{m} \tag{2.22}$$

Applying Newton's method, our approximate solution to Eq. (2.22) can be recovered with the formula:

$$X_{n+1} = X_n - [F'(X_n)]^{-1} F(X_n) \tag{2.23}$$

where, $F(X_{n+1}) = \begin{bmatrix} f_1(X_{n+1}) & f_2(X_{n+1}) \end{bmatrix}^T$, and

$$F(X_{n+1}) = \begin{bmatrix} f_1(X_{n+1}) \\ f_2(X_{n+1}) \end{bmatrix} = \begin{bmatrix} s_{n+1} - s_n - \Delta t v_{n+1} \\ v_{n+1} - v_n - \Delta t \left(\frac{F_0}{m} e^{-\frac{s_{n+1}}{L}} - \frac{k}{m} s_{n+1} - \mu_d \frac{W_0}{m} \right) \end{bmatrix}$$

$F'(X_{n+1})$ is the Jacobian of the nonlinear residual as given in Eq. 2.24.

$$F'(X_{n+1}) = \begin{bmatrix} \frac{\partial f_1}{\partial s} & \frac{\partial f_1}{\partial v} \\ \frac{\partial f_2}{\partial s} & \frac{\partial f_2}{\partial v} \end{bmatrix} = \begin{bmatrix} 1 & -\Delta t \\ A & B \end{bmatrix}, \tag{2.24}$$

where $A = \Delta t [F_0 e^{-s/l} + kL] / (mL)$ and $B = 1$. By solving Eq. 2.23 iteratively with the help of a Matlab™-based Newton solver, the results plotted in Fig. 2.5 were obtained.

2.4.2.1 Modeling input parameters

The input parameters used to test the theoretical models were chosen to enable direct comparison with our experiments and are shown in Table 2.4.

Table 2.4: Modeling parameters for exponentially decreasing force with drag and boundary friction in the presence of a spring

Final Time	T	1 second
Object mass	m	1 kg
Applied Force	F_0	10.9 N
Normal Force	F_n	9.8 N
Initial velocity	u_0	0.001 m/s
Initial sliding distance	s_0	0.001 m
Friction Coefficients	μ	[.01; .05; .1]
Spring Constant	k	83 N/m
Length	L	.95

2.4.2.2 Results

The illustrative modeling results shown in Figs. 2.5a to 2.5d were plotted using Matlab™ software.

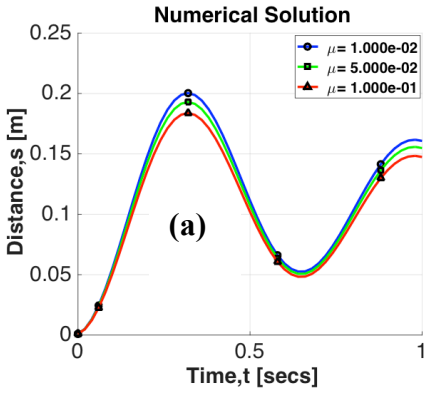

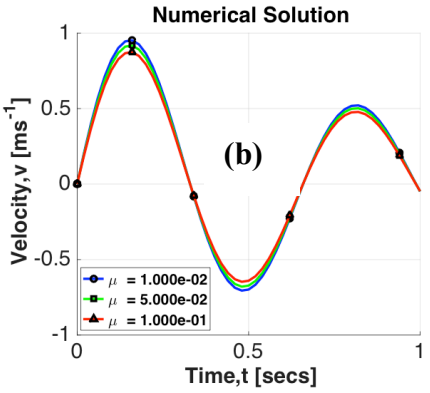

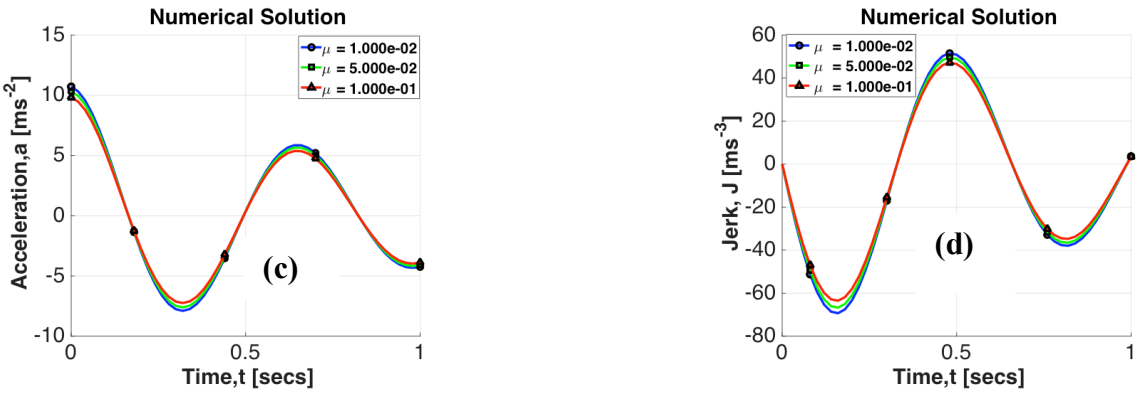

Figure 2.5: Effects of boundary friction on spring-loaded sliding objects when applied force exponentially decreases: (a) Sliding Distance, (b) Sliding Velocity, (c) Sliding Acceleration, (d) Sliding Jerk

2.4.3 Discussion of results

From the graphs, the following observations were made:

1. Three different friction coefficients corresponding to three constant friction forces were used in interrogating the modeling results. As can be seen from Figs. 2.4a and 2.5a, for the lowest friction coefficient, the highest distance is covered. Distance gradually increases from zero and gradually decreases again like sine waves. For a constant applied force, while decreasing, it goes down to zero but for a variable force, the range of maximum and minimum value decreases with time.
2. Figures 2.4b and 2.5b show that velocity is also affected by friction. The lower the friction coefficient, the higher the velocity. Velocity starts from zero, gradually increases and decreases to a negative value. Like distance, the range of maximum value and minimum value decreases with time under variable force.
3. Acceleration and jerk are also adversely affected by friction as can be seen from Figs. 2.4c, 2.4d, 2.5c and 2.5d. Acceleration starts from a positive value and reduces to a

negative value. Jerk behaves exactly oppositely to velocity. Starting from zero, jerk decreases to a negative value and then increases up to a positive value.

Chapter 3

Experimental Studies on Boundary Resisted Motion

To reconcile the theoretical modeling of boundary-resisted motion with experiments, a few experimental tests were conducted. The objectives of the experimental studies were to: 1) elucidate how the frictional resistances affect relative motion, and 2) decipher how friction coefficient behaves spatiotemporally. In classical mechanics theory, friction coefficient has always been assumed to be positive and constant but is friction coefficient really always constant and positive? To find out, we performed experiments for two different cases with each having two subcases just like we did in our theoretical modeling. Two sets of experiments Experiment 1 and Experiment 2 were ran.

Experiment 1:

We examined the effect of drag and solid boundary friction on the motion of the sliding object. Furthermore, this prototypical example was divided into two subcases:

a) Experiment 1A: Constant applied force

b) Experiment 1B: Exponentially decreasing force

Experiment 2:

In the second experiment, we examined the effects of boundary friction on a spring-loaded sliding object. As done previously, the second experiment was split into two subcases:

a) Experiment 2A: Constant applied force

b) Experiment 2B: Exponentially decreasing force

3.1 Experimental setup

The equipment used for the experiment is from Vernier Software & Technology. A schematic diagram of the experimental setup is shown in Fig. 3.1. An applied force F_a from a known weight slung over a pulley moves a block of mass m that carries an external load F_n. The block motion is opposed by an attached spring with force F_{sp} and boundary friction force F_{Bf} at the interface of the sliding block and a stationary block on which the block slides.

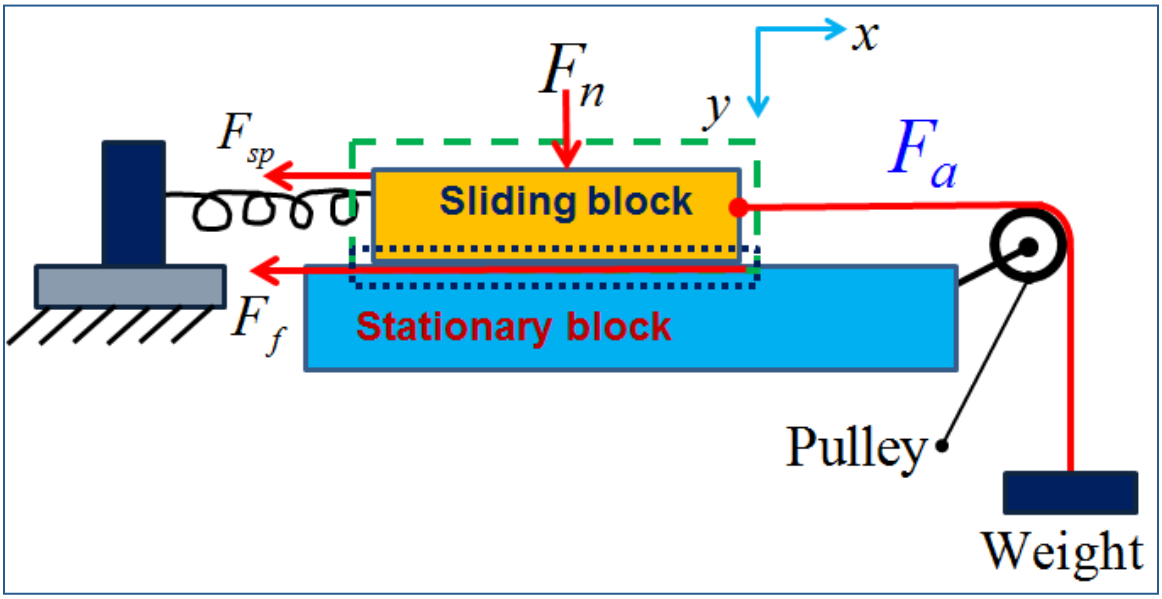

Figure-3.1: Experimental Setup

3.1.1 List of equipment

The pieces of equipment used in conducting the experiments are listed below:

1. 1 m track
2. 1 cart of .5 kg,
3. 4 masses with .125 kg,
4. A pulley

5. A spring of .09 m
6. A dual-range force transducer was used which can measure up to 50 N
7. Motion encoder receiver- to determine the position, velocity, acceleration and jerk

Photographs of key pieces of experimental apparatuses are shown in Figs. 3.2 to 3.4.

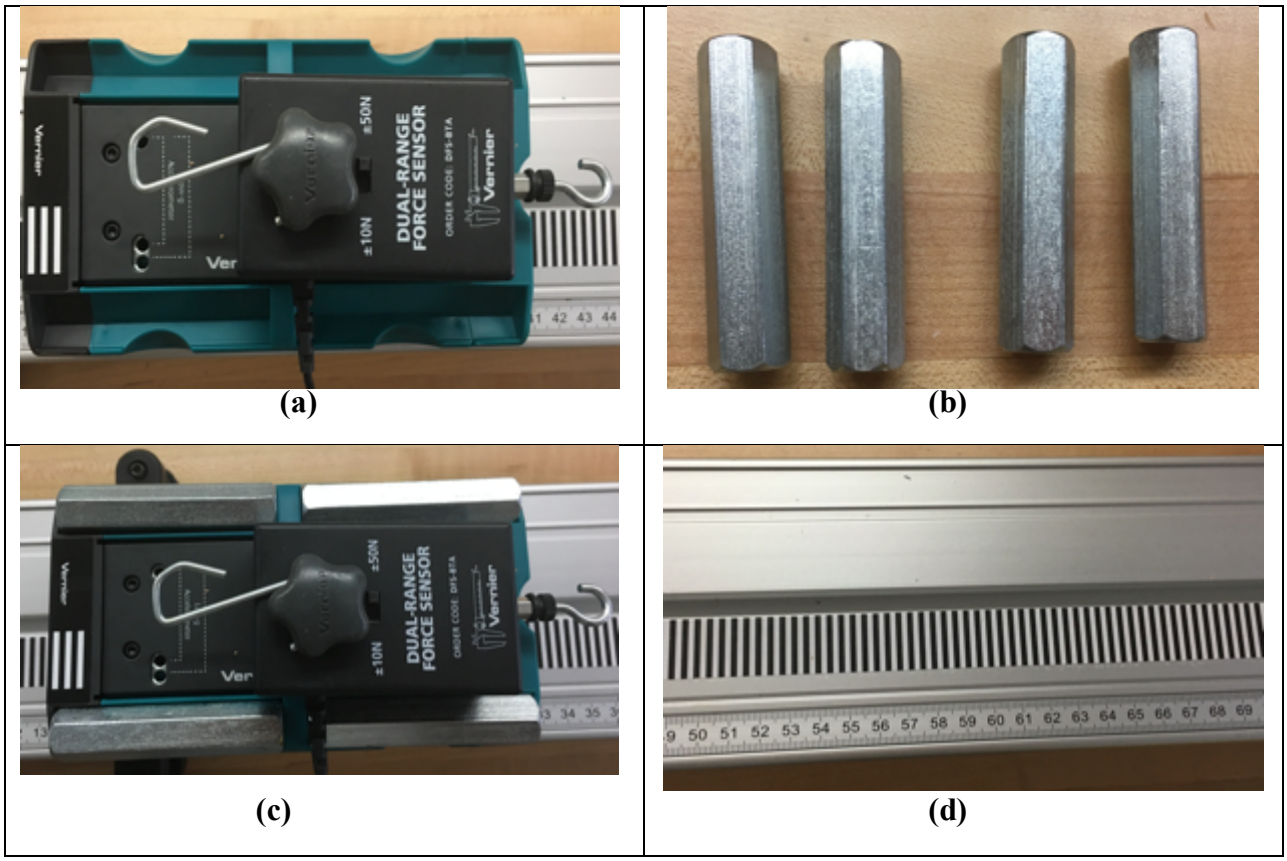

Figure-3.2: (a) Cart with force transducer attached to it, (b) masses of .125 Kg (c) cart with masses and dual range force transducer, (d) 1 meter track

(a)

(b)

(c)

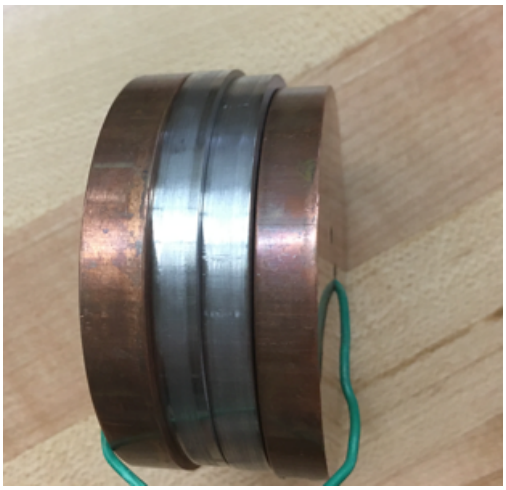

(d)

(e)

Figure-3.3: (a) Lab quest- data collection device (b) Motion encoder receive (c) Pulley, (d) Hanging mass of 1 kg, (e) Spring

3.1.2 Experimental Procedure

The experiment was conducted to determine instantaneous boundary friction force. To find instantaneous boundary friction force we considered two different cases for which we have already modeled and obtained analytical results. The first case was to observe how boundary friction behaved with a powered vehicle moving horizontally with constant and variable force. For this case, an analogous cart with masses was pulled and the horizontal pulling force determined using the dual- range force transducer. To apply a constant force, the cart was pulled with a fixed hanging mass of 1 kg attached to a pulley. To have a better understanding of boundary friction, a simple spring whose constant was determined by Hooke's Law.

$$\text{Spring Constant} = \frac{\text{Applied Force}}{\text{Length of Elongation}}$$

By keeping one end of the spring constant and attaching another end to the cart, the cart was pulled by the hanging mass of 1 kg hanging by means of a rope over the pulley for a constant applied force. Contrarily, to apply a variable force the pulley was pulled by hand while the dual range force transducer recorded the applied force.

3.1.3 Key experimental protocols

1. The experimental measurements were repeated at least four times to ascertain repeatability of the results.
2. The experimental accuracy for each measurements was observed using the in- built statistical tool of Vernier Software & Technology.

3.1.4 Uncertainty Analysis

Uncertainty Analysis is very important for experimental designs and demonstrates the relative accuracy of experimentally measured quantities. The uncertainty in a measured quantity affects and is propagated through the measurements of other variables directly affecting the desired measured value. Standard methods for calculating experimental uncertainty is widely documented for example see reference [69]. Consider a measured experimental quantity R which is depending on several independent variables $x_1, x_2, \ldots, x_n$ where $R = R(x_1, x_2 \ldots\ldots x_n)$ [69]. The uncertainty in each independent variable $u_1 u_2, \ldots, u_3$ leads to the cumulative uncertainty u_R as given in Eq. 3.1.

$$u_R = \pm\left[\left(\frac{x_1}{R}\frac{\partial R}{\partial x_1}u_1\right)^2 + \left(\frac{x_2}{R}\frac{\partial R}{\partial x_2}u_2\right)^2 + \ldots + \left(\frac{x_n}{R}\frac{\partial R}{\partial x_n}u_n\right)^2\right]^{1/2} \tag{3.1}$$

In the experimental results, the Logger Pro™ software was used, which automatically calculated the uncertainty associated with all the measured data. The built-in uncertainty calculator gave the uncertainty propagation analyses for two experimental case studies. The uncertainties associated with each measured response are summarized in Table 3.1 and illustrated as error bars in Figs. 3.1 to 3.24.

Table 3.1: Uncertainty Analysis

Case Study	**Case Study-1 Subcase -1A**	**Case Study-1 Subcase -1B**	**Case Study-2 Subcase -2A**	**Case Study-2 Subcase -2B**
Sliding Distance	± .02741	± 0.001290	± 0.01184	± 0.01749
Sliding Velocity	± 0.177	± 0.002893	± 0.05027	± 0.08323
Sliding Acceleration	± 1.169	± 0.009454	± 0.4533	± 1.081

Sliding Jerk	± 16.85	± 0.2252	± 3.391	± 11.79
Coefficient of friction	± 0.08949	± 0.0007235	± .1850	± .04979

3.2 Experiment 1: Effects of boundary friction on drag-resisted horizontal motion

3.2.1 Experiment 1A: Constant applied force with drag and boundary friction

In this subcase, the cart was pulled by a constant applied force of 7.35 N by the help of a pulley and a hanging mass of .75 Kg. The experimental results showing temporal kinematic properties were recorded. Distance, velocity, acceleration and jerk were measured using the motion encoder receiver and force was measured with the dual range force transducer. The accompanying LabQuest™ software automatically recorded all the results, which were exported to Excel™ for post processing. The modeling parameters are used as below-

Table 3.2: Modeling parameters for constant applied force with drag and boundary friction

Final Time	T	1.2 seconds
Object mass	m	1 kg
Constant Applied Force	F_a	7.5 N
Normal Force	F_n	9.8 N
Air Density	ρ	1.225 kg/m^3
Drag Coefficient	C_D	1.2
Initial velocity	u_0	0 m/s
Initial sliding distance	s_0	0.001 m

Area	A	.095 m *.035 m
Friction Coefficients	μ	[.7; .65; .6]

3.2.1.1 Results:

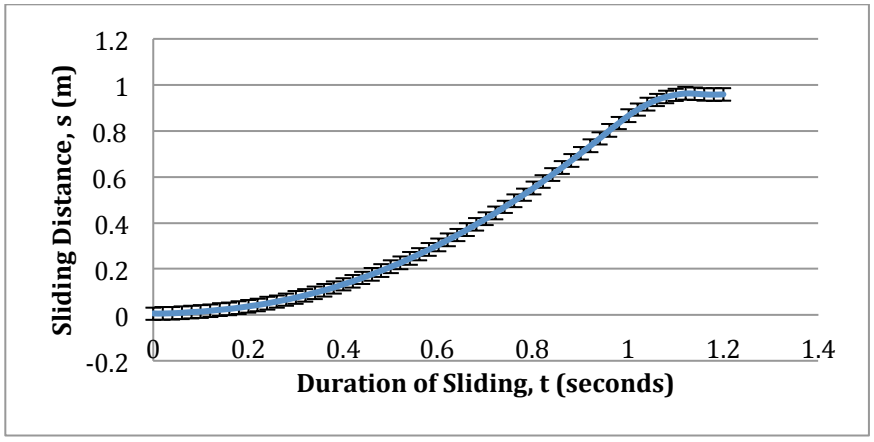

Figure 3.4- Effects of boundary friction on sliding distance when applied force is constant

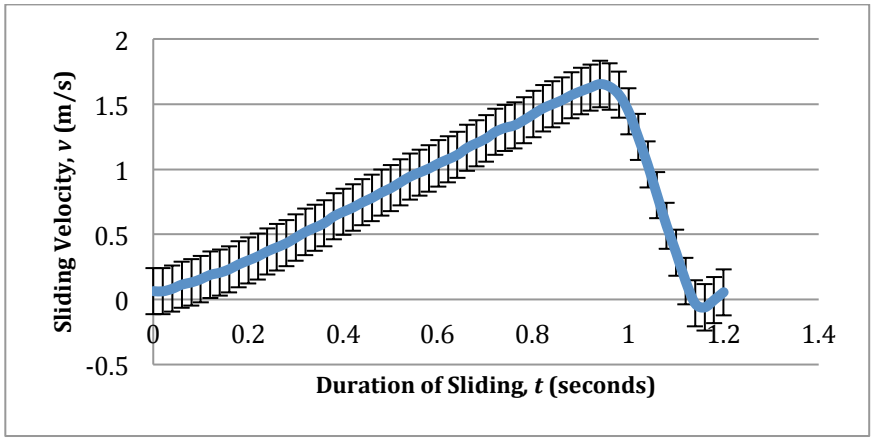

Figure 3.5- Effects of boundary friction on sliding velocity when applied force is constant

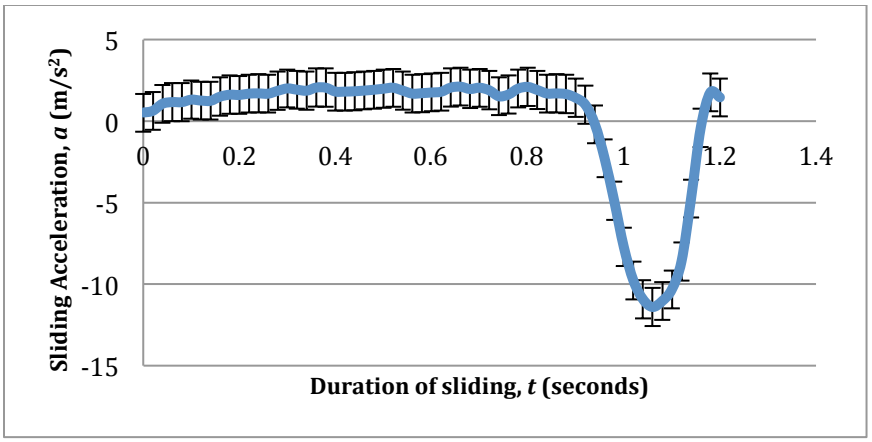

Figure 3.6- Effects of boundary friction on sliding acceleration when applied force is constant

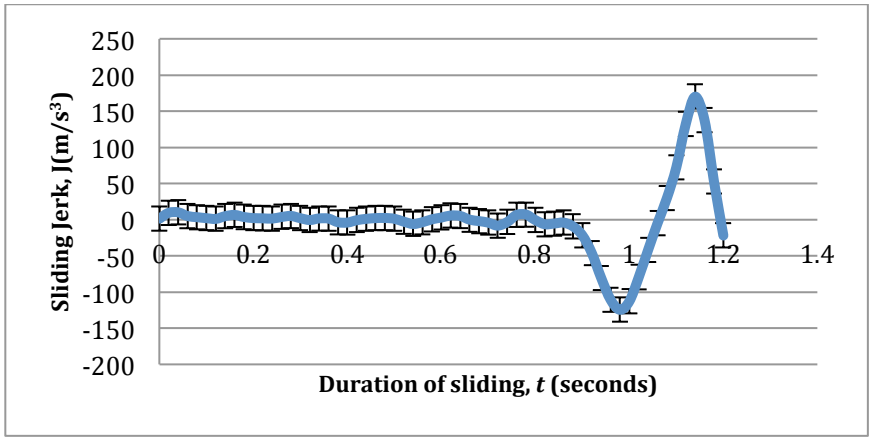

Figure 3.7- Effects of boundary friction on sliding distance when applied force is constant

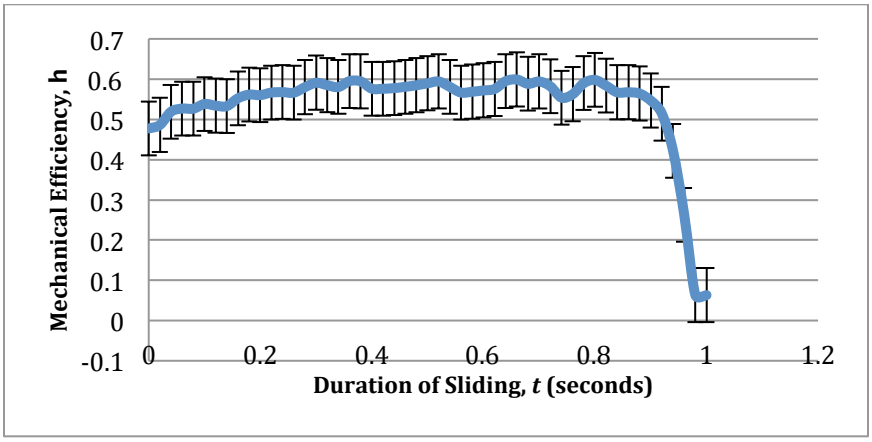

Figure 3.8- Effects of boundary friction on mechanical efficiency when applied force is constant

3.2.1.2 Extracting frictional behavior experimentally

From the measured mechanical responses and using Newton's 2nd law from Eq. 2.1, the instantaneous coefficient of friction, μ was calculated.

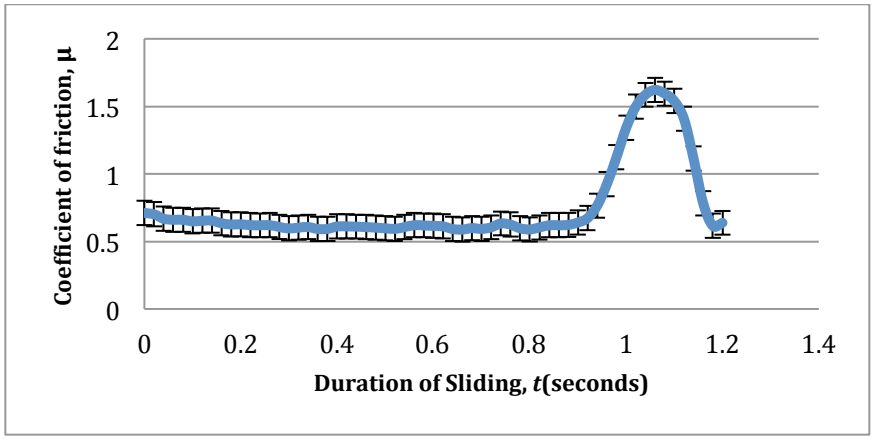

Figure 3.9- Effects of boundary friction on coefficient of friction on sliding object when applied force is constant

3.2.1.3 Discussion of results

From the plotted experimental results, the following deductions were made:

1. As it can be seen from Fig. 3.4, after 1 second the distance is not increasing anymore. It can therefore be understood that the cart stops.
2. Until 1 second elapses, the distance is almost increasing at a constant rate. That explains why from Fig. 3.5, velocity is increasing at an almost constant rate with time up to 1 second and then it drops down to zero.
3. Since velocity is increasing at a constant rate, Fig. 3.6 shows how acceleration remains almost constant and Fig. 3.7 indicates that jerk is zero.

4. While observing the behavior of the instantaneous coefficient of friction μ, as in Fig. 3.9, it is clear that coefficient of friction is not constant. Although μ varies, the variation seems only slight. And at the end the instantaneous friction coefficient increases significantly as the cart gradually stops.
5. Figures 3.8 and 3.9 capture how coefficient of friction directly affects mechanical efficiency. Mechanical efficiency is inversely proportional to coefficient of friction. As the cart stops, the coefficient of friction suddenly increases and mechanical efficiency suddenly decreases.

3.2.2 Experiment 1B: Exponentially decreasing force with boundary friction

In the second experiment, the cart was pulled by an initial force of 0.95 N. Results capturing instantaneous kinematic responses like distance, velocity, acceleration and jerk were measured with the motion encoder receiver. Additionally, the applied force was measured with the dual range force transducer. The recorded results were exported from the LabQuest™ for post processing in Excel™.

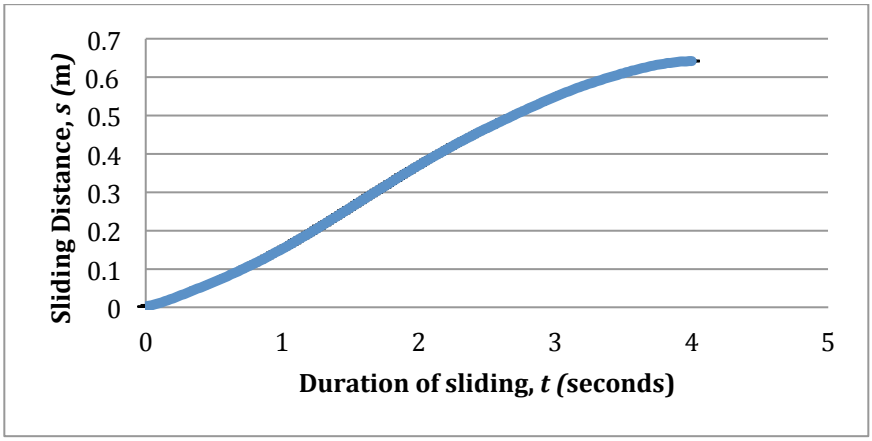

Figure 3.10- Effects of boundary friction on sliding distance when applied force exponentially decreases

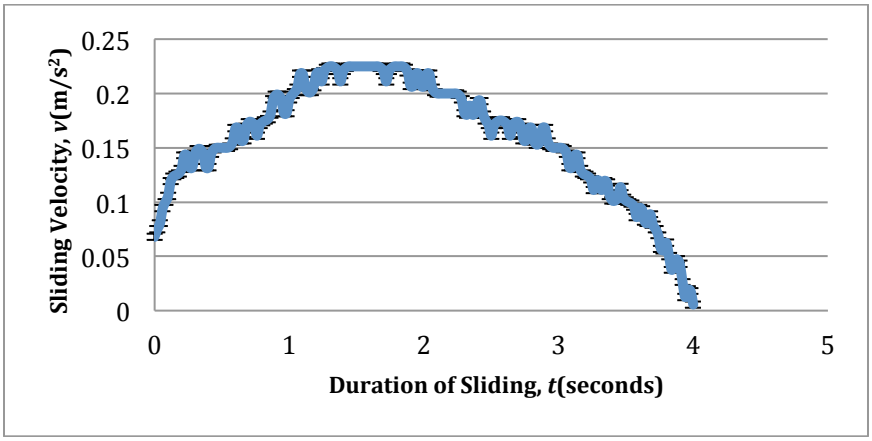

Figure 3.11- Effects of boundary friction on sliding velocity when applied force exponentially decreases

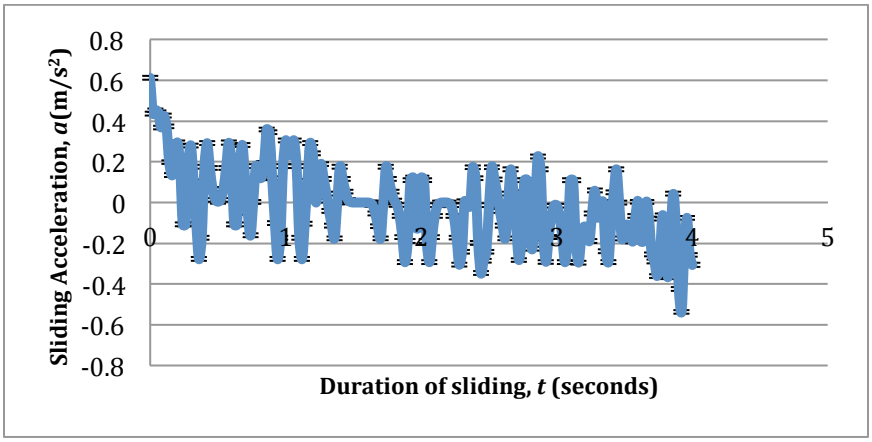

Figure 3.12- Effects of boundary friction on sliding acceleration when applied force exponentially decreases

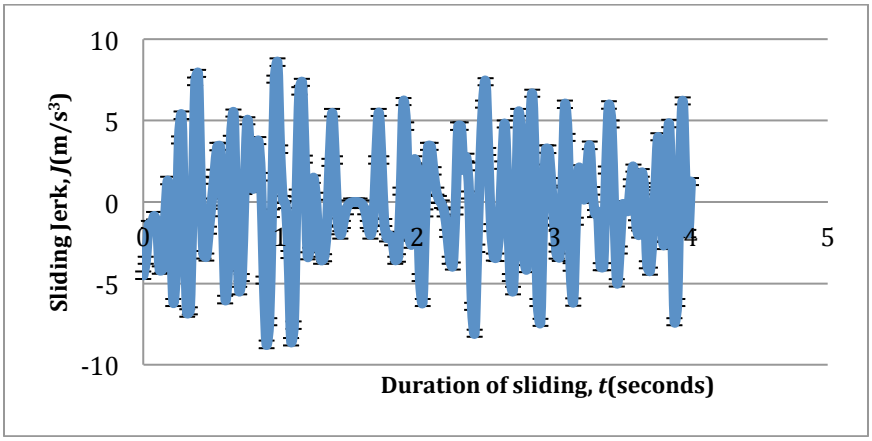

Figure 3.13- Effects of boundary friction on sliding jerk when applied force exponentially decreases

3.2.2.1 Extracting frictional behavior experimentally

From the measured mechanical responses and using Newton's 2nd law from Eq. 2.14, the instantaneous coefficient of friction was obtained.

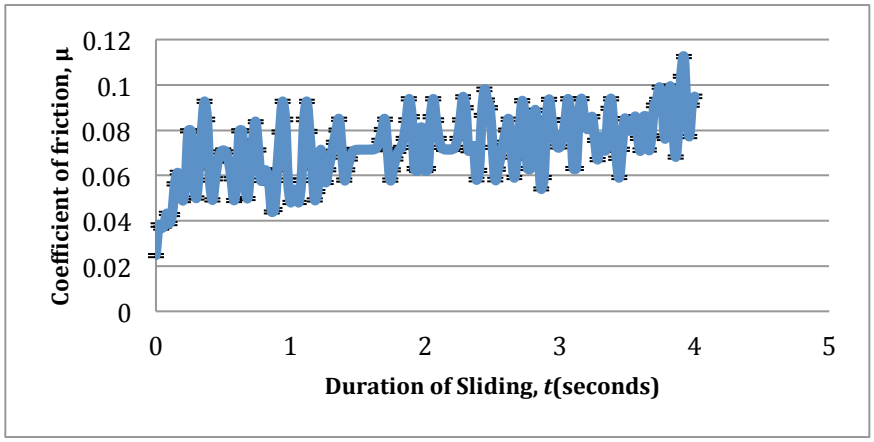

Figure 3.14- Effects of boundary friction on coefficient of friction on sliding object when applied force exponentially decreases

3.2.2.2 Discussion of results

From the graphically illustrated experimental results, the following deductions were made:

1. The results are not as stable as for the case with a constant applied force.
2. As the initial applied force was as low as 0.95 N, the cart takes almost 4 seconds to cover a distance 0.6 m as depicted by Fig. 3.10.
3. As can be seen from Fig. 3.11, after 4 seconds, the velocity reduces to zero. It can then be understood that the cart stopped after 4 seconds.

4. The velocity increases gradually from 0.075 m/s to a maximum value of 0.21 m/s at 1.38 seconds and the gradually decreases to zero at 4 seconds. Since velocity fluctuates, it may explain why from Figs. 3.12 and 3.13 instantaneous acceleration and jerk also fluctuate.
5. Figure 3.14 shows the instantaneous coefficient of friction. The fluctuations noticeable in velocity may account for the major fluctuation in instantaneous coefficient of friction. At 0.02 seconds, the coefficient of friction is 0.03 which then increases to 0.1 at the end of four seconds.

3.3 Case Study-2: Influence of boundary friction on a spring loaded sliding object

3.3.1 Subcase-2A: Constant applied force with boundary friction

In this experiment subcase one end of the spring was fixed while the other end was attached to the cart. A constant applied force of 9.3 N pulled the other end of the cart with the 0.95 kg hanging mass attached over the pulley. The instantaneous kinematic properties of distance, velocity, acceleration and jerk were measured with the motion encoder receiver while the applied force was measured with dual range force transducer. The measured results were exported from the LabQuest™ software to Excel™ for post processing.

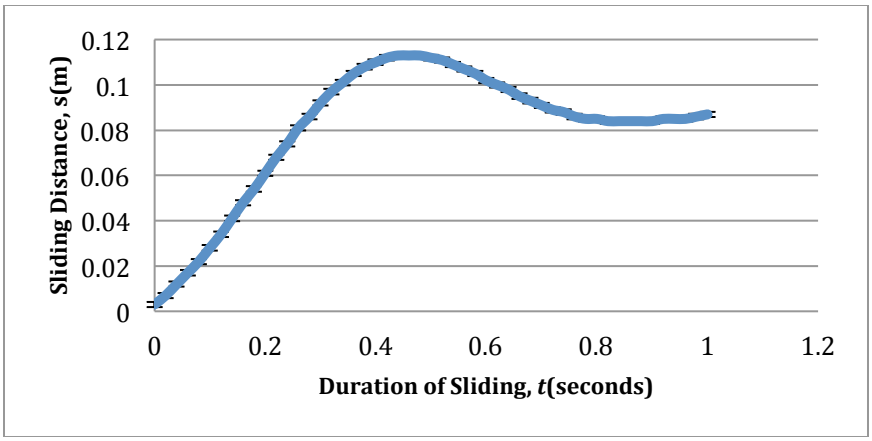

Figure 3.15- Effects of boundary friction on sliding distance when applied force is constant

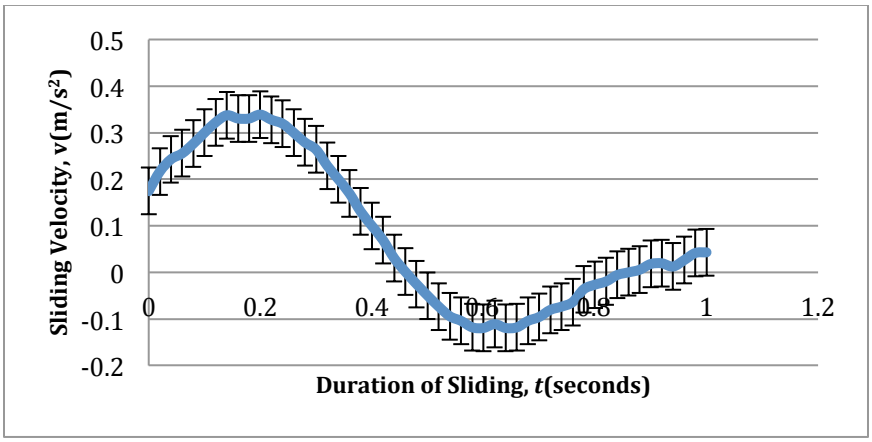

Figure 3.16- Effects of boundary friction on sliding velocity when applied force is constant

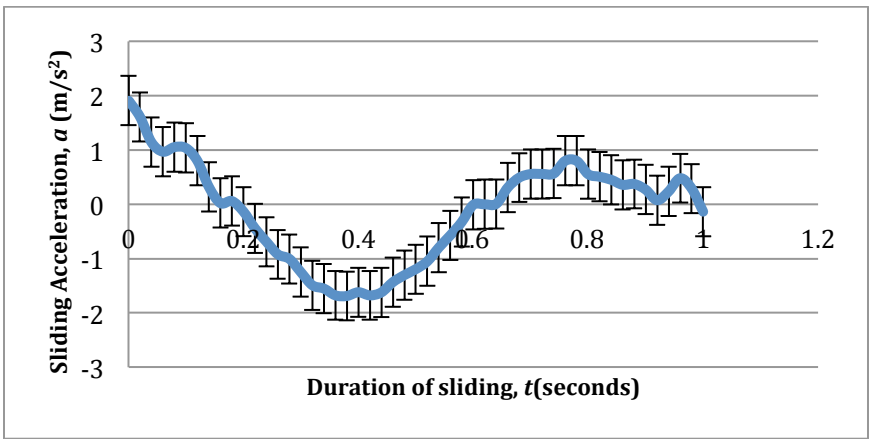

Figure 3.17- Effects of boundary friction on sliding acceleration when applied force is constant

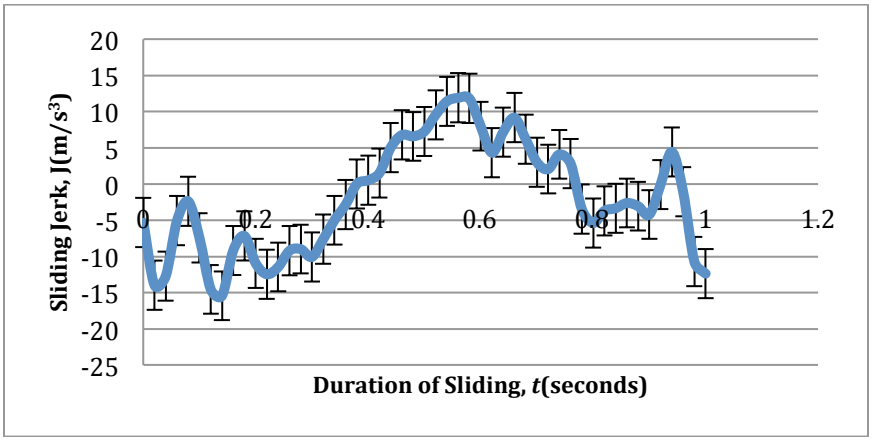

Figure 3.18- Effects of boundary friction on sliding jerk when applied force is constant

3.3.1.1 Extracting Frictional Behavior experimentally

From the measured mechanical responses and using Newton's 2nd law from Eq. 2.17, the instantaneous coefficient of friction was calculated.

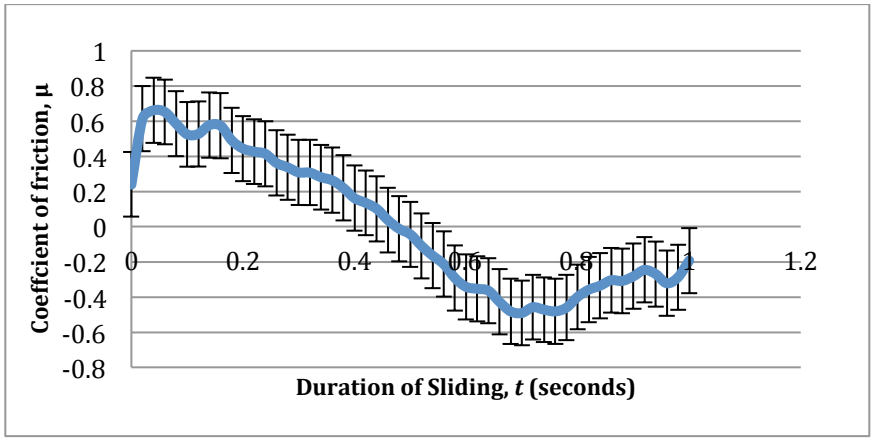

Figure 3.19- Effects of boundary friction on coefficient of friction on sliding object when applied force is constant

3.3.1.2 Discussion of results

From the graphs plotted illustrating the experimental results, the following observations were made:

1. Since a spring was attached to one end of the cart, it can be deduced from Fig. 3.15 that the cart moves forwards and backwards. The maximum distance covered is about 0.11 m.
2. As can be seen from Fig. 3.16, after gradually increasing to 0.33 m/s, the velocity reduces to a negative value as the cart moves through a negative distance.
3. Figure 3.17 shows that acceleration moves through a negative value before increasing. There is a noticeable fluctuation in acceleration values, which was captured in Fig. 3.18 as instantaneous jerk. Jerk starts from a negative value before gradually increasing.
4. As can be seen from Fig. 3.19, the instantaneous coefficient of friction seems to correspond to the instantaneous velocity from Fig. 3.16. It can also be seen that the instantaneous friction coefficient even becomes negative capturing how the cart moves backwards rather than forwards. In this case the instantaneous friction is now acting in the reverse direction in complete agreement with the nature of friction as always opposing the direction of motion.

3.3.2 Subcase-2B: Exponentially decreasing force with boundary friction

In this subcase, one end of the spring was fixed while the other end was attached to the cart. An initial applied force of 10.9 N pulled the other end of the cart. The instantaneous kinematic properties of distance, velocity, acceleration and jerk were measured using the motion encoder receiver while the applied force was measured with

the dual range force transducer. The measured experimental results were exported from LabQuest™ to Excel™ for post processing.

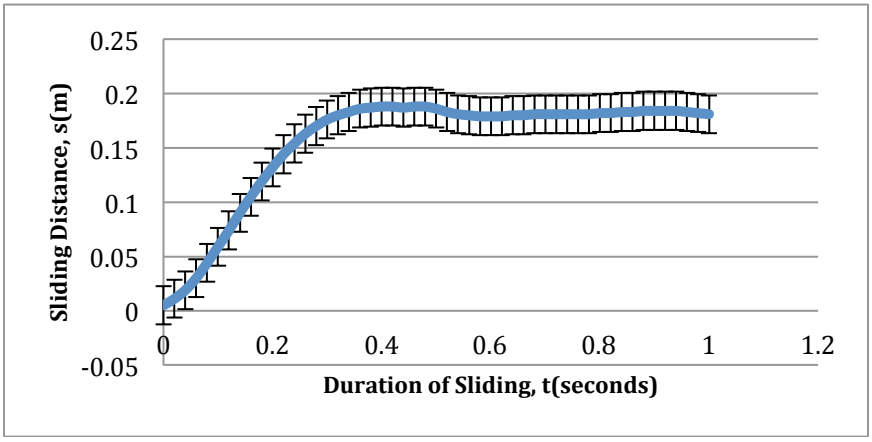

Figure 3.20- Effects of boundary friction on sliding distance when applied force exponentially decreases

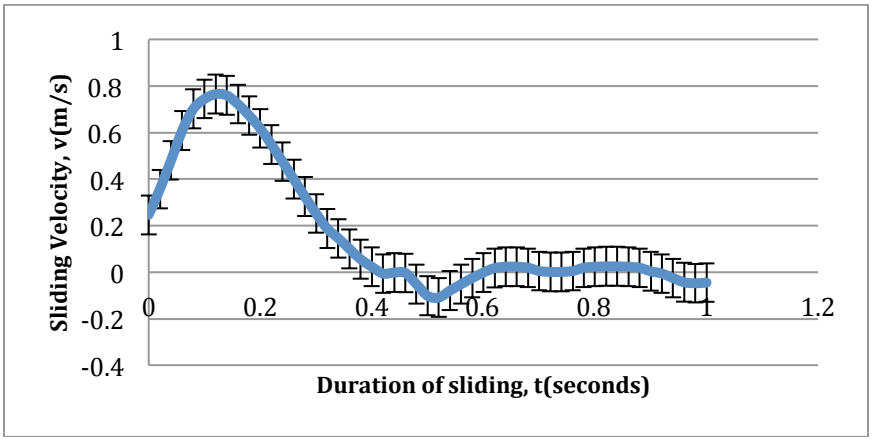

Figure 3.21- Effects of boundary friction on sliding velocity when applied force exponentially decreases

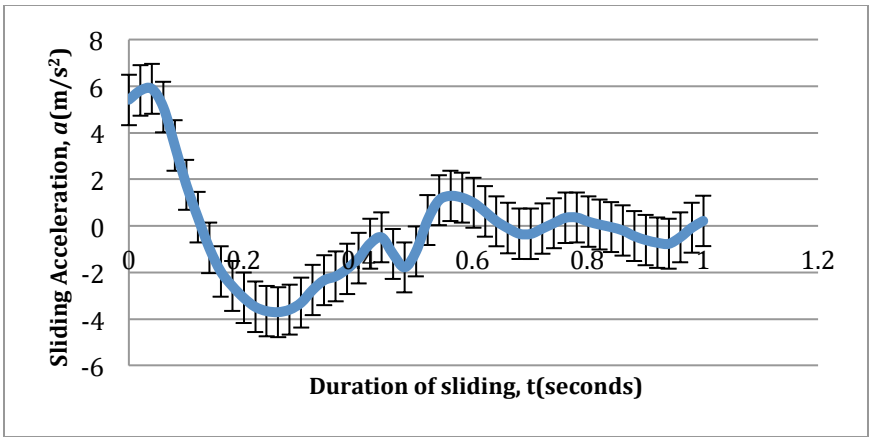

Figure 3.22- Effects of boundary friction on sliding acceleration when applied force exponentially decreases

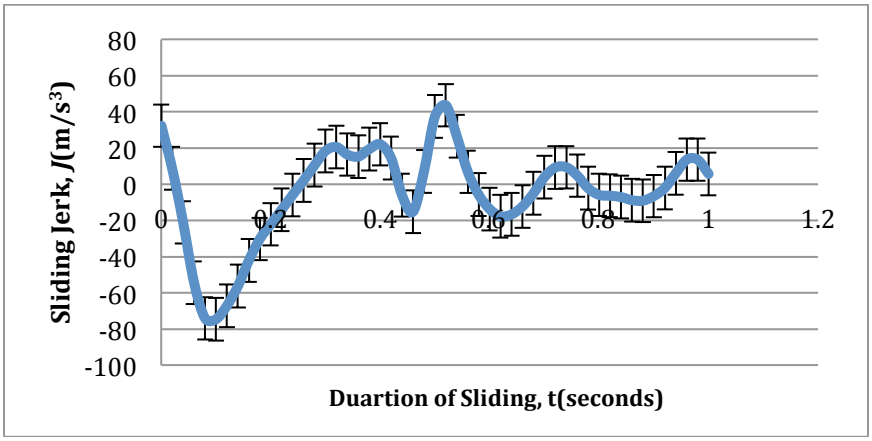

Figure 3.23- Effects of boundary friction on sliding jerk when applied force exponentially decreases

3.3.2.1 Extracting Frictional Behavior experimentally

From the measured mechanical responses and using Newton's 2nd law from Eq. 2.22, the instantaneous coefficient of friction was quantified.

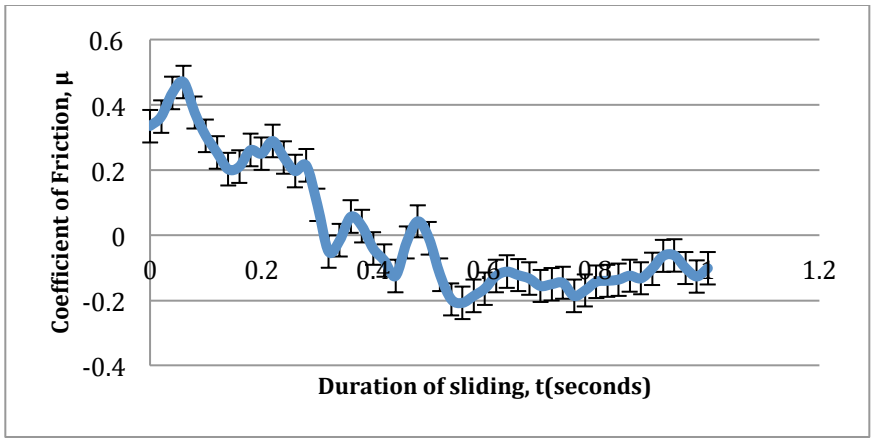

Figure 3.24- Effects of boundary friction on coefficient of friction on sliding object when applied force exponentially decreases

3.3.2.2 Discussion of results

From the plotted experimental results, the following observations were made:

1. Since one end of the spring was attached to one end of the cart, it can be observed from Fig. 3.20 that the cart moves forward and backwards. The maximum distance covered was about 0.18 m
2. From Fig. 3.21, after gradually increasing to 0.76 m/s, the velocity reduces to a negative value as the cart covers a negative distance backwards.
3. Figure 3.22 shows that acceleration moves through a negative value before increasing.
4. Figure 3.23 shows how instantaneous jerk gradually decreases to a negative value and before subsequently increasing.
5. As shown in Fig. 3.24, the instantaneous friction coefficient fluctuates significantly. Furthermore, it can be seen that the instantaneous friction coefficient becomes negative showing the cart moving backwards rather than forwards. In other words,

friction acts in a reverse direction as expected since friction always acts in the direction opposing motion.

Chapter 4

Comparison Between Theoretical and Experimental Results

From scientific, engineering, and technical literature, we find that there is much intellectual capital to be gained by providing a theoretical framework wherein basic friction-based dynamic modeling is compared with experiments [3, 45, 55, 70]. This way, by inferring an appropriate deterministic friction model, a friction-based mechanical efficiency protocol can be constructed. This deterministic approach will complement thermodynamic schemes synthesizing engine dissipations resulting from irreversibility [71-74]. Schemes for proposing fuel standards will benefit from first principles-based frictional dissipations of efficiency without overly relying on heuristic approaches [9, 75-81].

From the experimental results of Chapter 3, two cases of boundary-resisted motion were studied. The experimental parameters comprising the mass of the cart, hanging mass, length of the track, spring constant, and applied force were measured and used as modeling input parameters interrogating the theoretical models. The instantaneous friction forces were measured from the experimental results using the interacting force equations in Eqs. 2.1, 2.14, 2.17, and 2.22. Since only constant boundary friction forces were used in the theoretical modeling, the experimental friction forces were averaged to facilitate direct comparison between experiments and modeling results.

In this chapter the applicable theoretical results and experimental results are compared. For our theoretical values we assumed our friction coefficient to be constant but for our experimental values, we saw that friction coefficients may vary within little range but it is not absolutely constant. Theoretical kinematic properties of distance, velocity, acceleration and jerk were compared to experimental results.

4.1 Case Study-1 vs. Experiment 1: Effects of boundary friction on drag-resisted horizontal motion

4.1.1 Subcase-1: Constant Applied force with drag and boundary Friction

The input modeling parameters are same as those used in Table 2.1 and 3.1. The friction coefficient we choose is 0.7. The uncertainties are shown for experimental results.

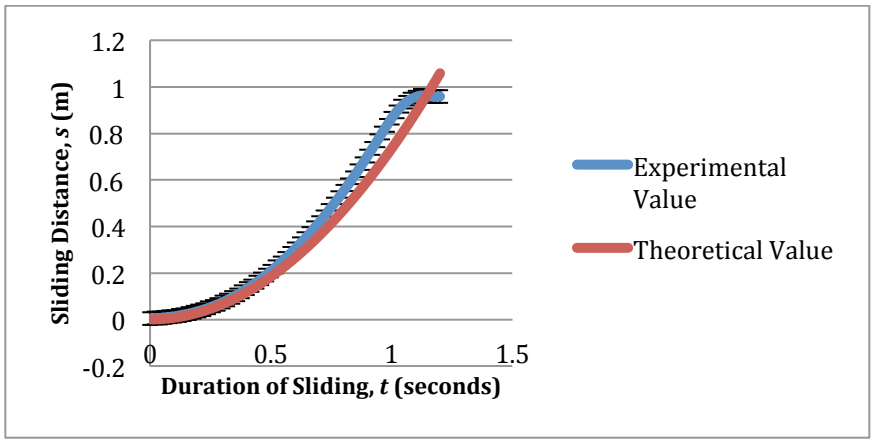

Figure 4.1- Effects of boundary friction on sliding distance for both theoretical modeling and experimental studies when applied force is constant

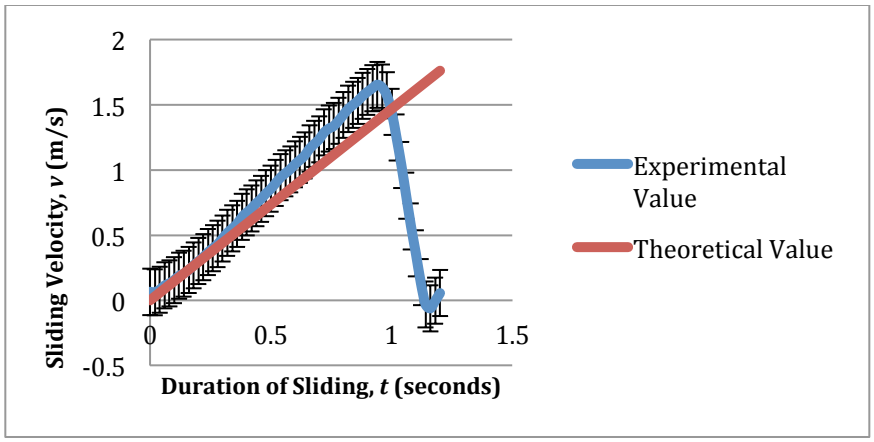

Figure 4.2- Effects of boundary friction on sliding velocity for both theoretical modeling and experimental studies when applied force is constant

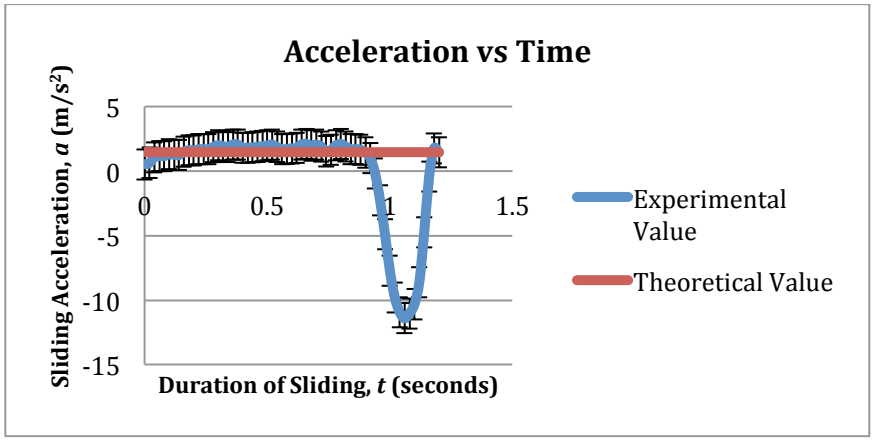

Figure 4.3- Effects of boundary friction on sliding acceleration for both theoretical modeling and experimental studies when applied force is constant

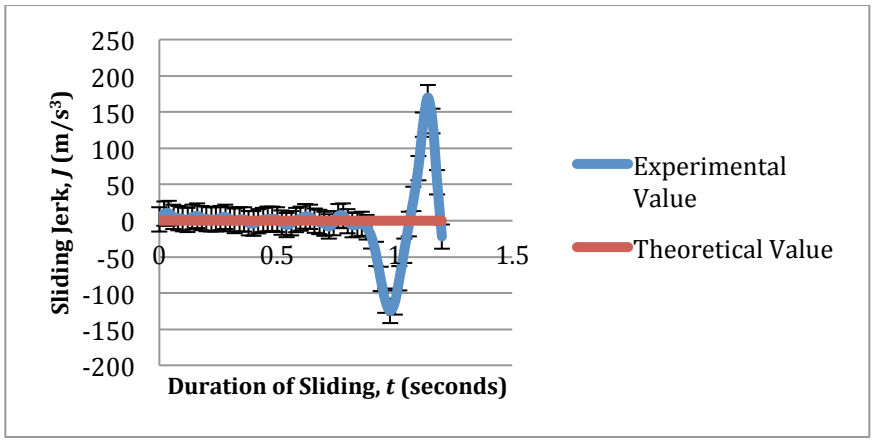

Figure 4.4- Effects of boundary friction on sliding jerk for both theoretical modeling and experimental studies when applied force is constant

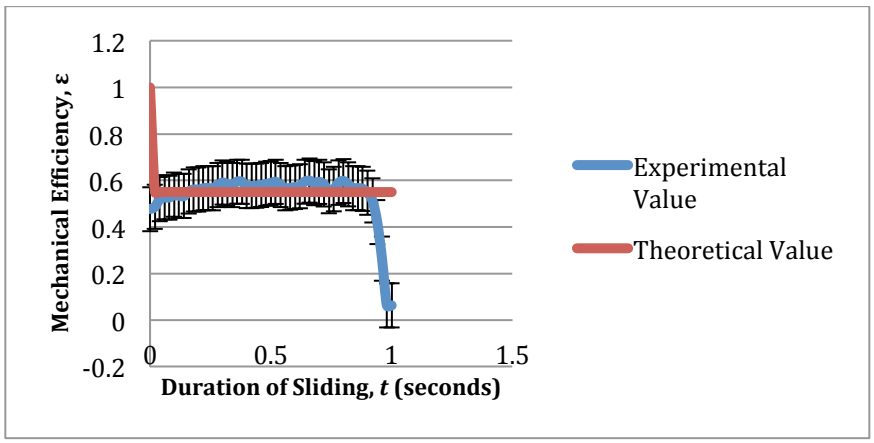

Figure 4.5- Effects of boundary friction on mechanical efficiency for both theoretical modeling and experimental studies when applied force is constant

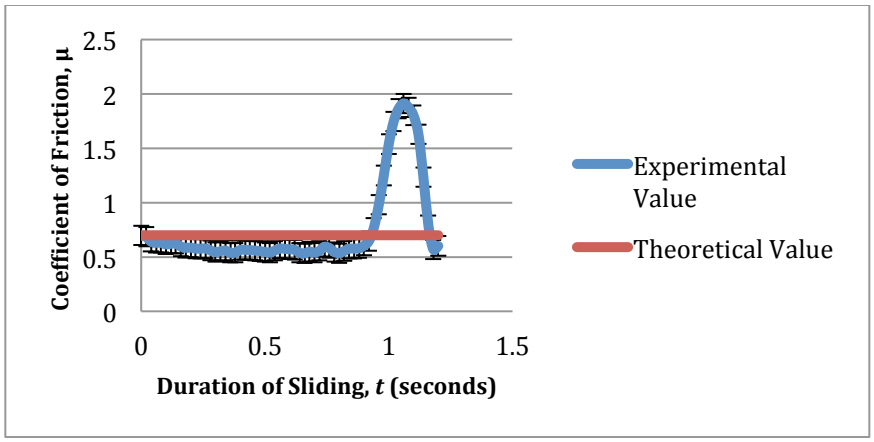

Figure 4.6- Effects of boundary friction on coefficient of friction for both theoretical modeling and experimental studies when applied force is constant

4.1.1.1 Discussion of results

1. From Fig. 4.1, it can be seen that the experimental and theoretical distances are almost similar. After 1 second, the instantaneous experimental distance becomes constant when the cart stopped while the theoretical instantaneous distance keeps increasing since the final time was taken as an input although the final theoretical distance was not fixed.
2. As can be seen from Fig. 4.2, the experimental velocity increases but reduces to zero for the stopping cart while the theoretical velocity increases constantly without a preconditioned stopping as expected.
3. Figure 4.3 shows the instantaneous experimental and theoretical accelerations. Since for theoretical velocity was increasing constantly, the theoretical acceleration expectedly remains constant. Contrarily the experimental acceleration is fluctuates dropping to a negative value as thereby capturing the deceleration as the cart comes to a stop.

4. It can be observed from Fig. 4.4 that instantaneous theoretical jerk is almost zero aligning with the constant theoretical acceleration. Contrarily, the experimental jerk fluctuates within values closer to zero but at the end it drops down and rises again to a positive value.
5. Figure 4.5 depicts experimental mechanical efficiency suddenly decreases at the end when the cart stops while the theoretical mechanical efficiency remained constant when instantaneous friction coefficient was constant.
6. From figure 4.6, we can see that while theoretical friction coefficient was constant, we can clearly see experimental friction coefficient increases at the end while the cart was stopping.
7. All the graphs show similar trends both for theoretical and experimental values, until at the end when the cart comes to a stop.

4.1.2 Subcase-2: Exponentially decreasing force with boundary friction

The input modeling parameters are same as those used Table 2.2. The friction coefficient chosen was 0.06.

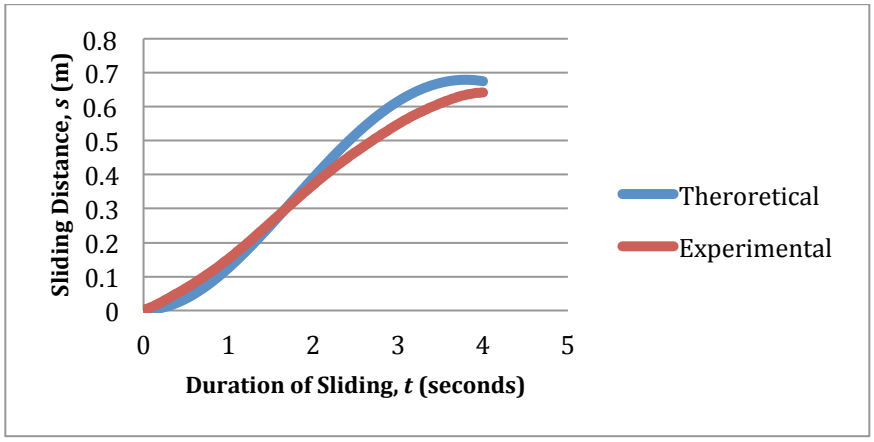

Figure 4.7- Effects of boundary friction on sliding distance for both theoretical modeling and experimental studies when applied force is decreasing exponentially

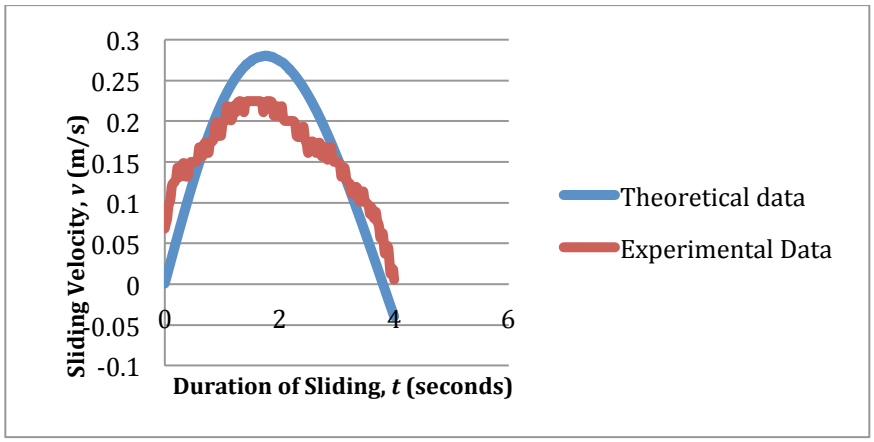

Figure 4.8- Effects of boundary friction on sliding velocity for both theoretical modeling and experimental studies when applied force is decreasing exponentially

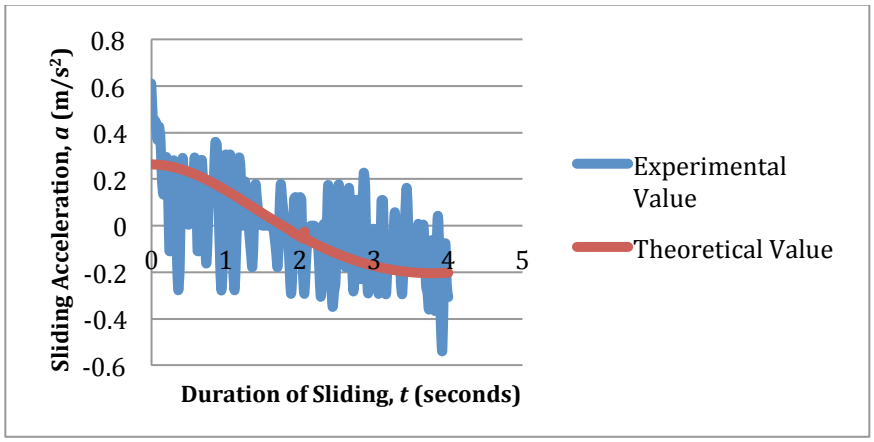

Figure 4.9- Effects of boundary friction on sliding acceleration for both theoretical modeling and experimental studies when applied force is decreasing exponentially

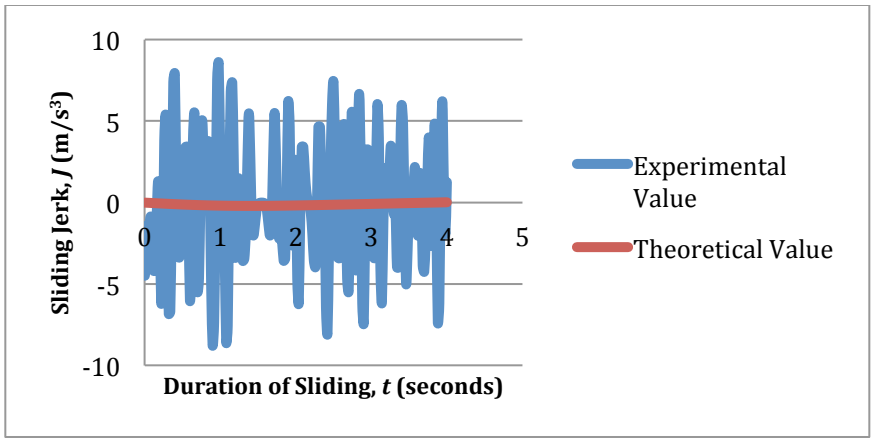

Figure 4.10- Effects of boundary friction on sliding jerk for both theoretical modeling and experimental studies when applied force is decreasing exponentially

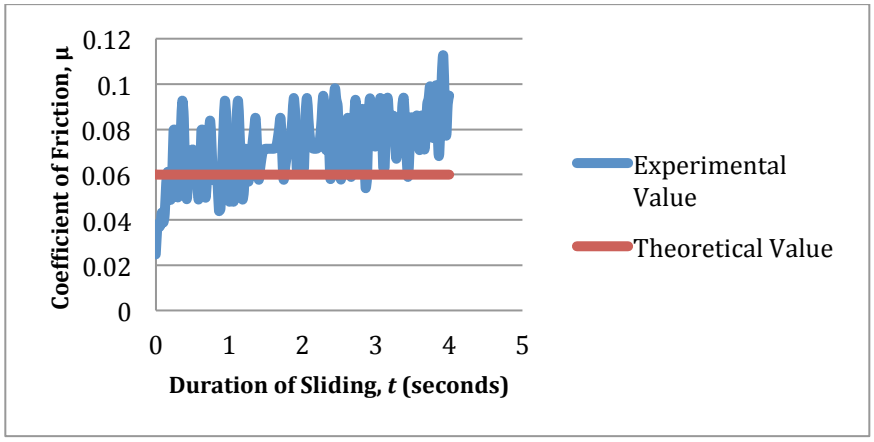

Figure 4.11- Effects of boundary friction on coefficient of friction for both theoretical modeling and experimental studies when applied force is decreasing exponentially

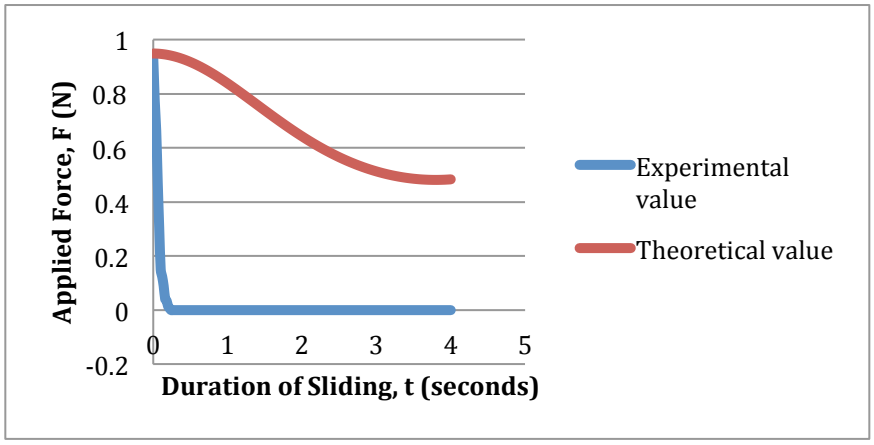

Figure 4.12- Effects of boundary friction on applied force for both theoretical modeling and experimental studies

4.1.2.1 Discussion of results

1. From Fig. 4.7, it can be seen that experimental and theoretical instantaneous distances are almost similar although the theoretical distance is higher than experimental distance at the end of 4 seconds.
2. As can be seen from Fig. 4.8, a stable theoretical velocity curve from our theoretical results was observed. Also, although experimental velocity follows a similar pattern, there are slight fluctuations.
3. Figure 4.9 shows instantaneous theoretical and experimental acceleration comparison. The theoretical acceleration starts from a positive value and goes down to a negative value. While experimental acceleration varies similarly there appear to be more noticeable fluctuations compared to the fluctuations of experimental velocity.
4. It can be observed closely from Fig. 4.9 that jerk is close to zero for theoretical values. But experimental jerk fluctuates a lot more than the experimental jerk for constant applied force. The range of jerk fluctuation is +9 m/s^3 to -9 m/s^3.
5. While theoretical friction coefficient is constant, we can clearly see experimental friction coefficient increases gradually with more fluctuations. However, for theoretical modeling, force is considered to be decreasing exponentially but experimentally same force is applied at first but force goes down to zero within a split of second.
6. From figure 4.12, it can be seen that, the exponentially decaying force that was considered for theoretical modeling was not the same for experiments. Because in experimental design, it was not possible to apply the same type of force. So the

mechanical responses that were observed for this case deviate from theoretical mechanical responses.

4.2 Case Study-2 vs. Experiment 2: Effects of boundary friction on spring-resisted horizontal motion

4.2.1 Subcase-1: Constant Applied force with boundary friction

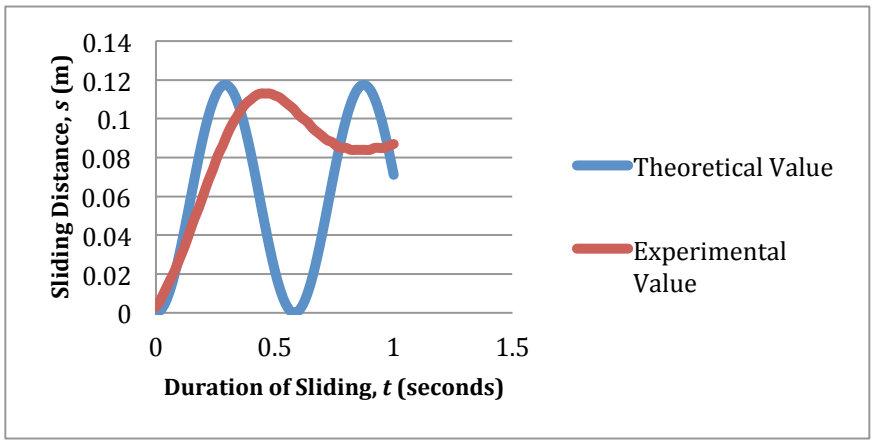

Figure 4.13- Effects of boundary friction on sliding distance for both theoretical modeling and experimental studies when applied force is decreasing exponentially

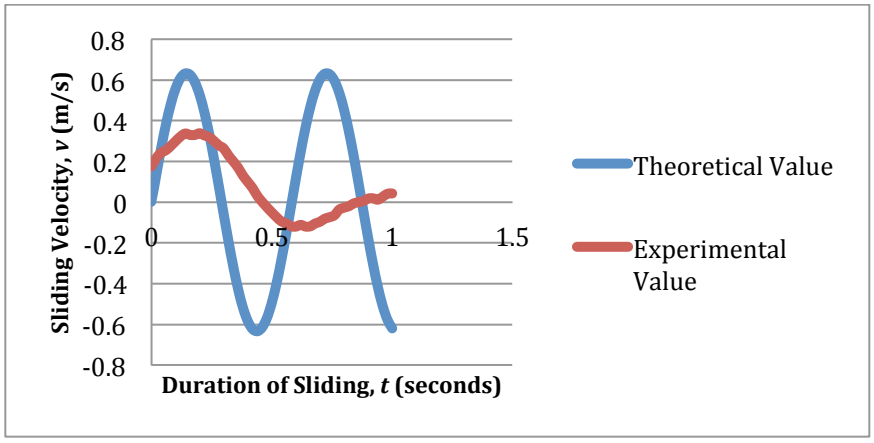

Figure 4.14- Effects of boundary friction on sliding velocity for both theoretical modeling and experimental studies when applied force is constant

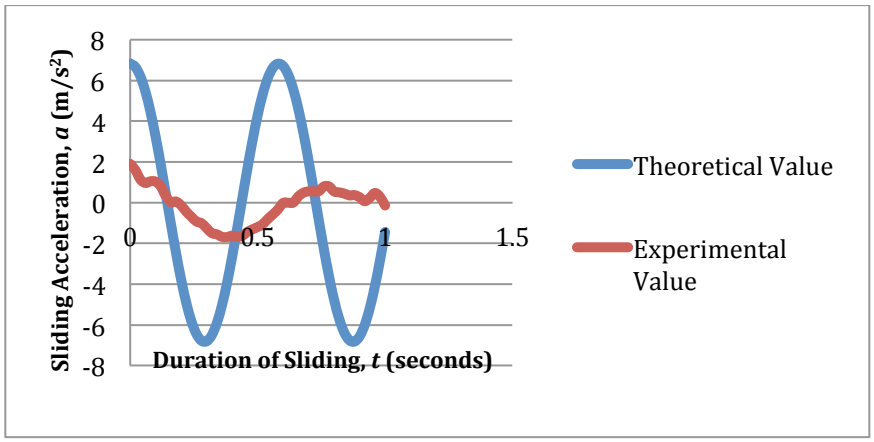

Figure 4.15- Effects of boundary friction on sliding acceleration for both theoretical modeling and experimental studies when applied force is constant

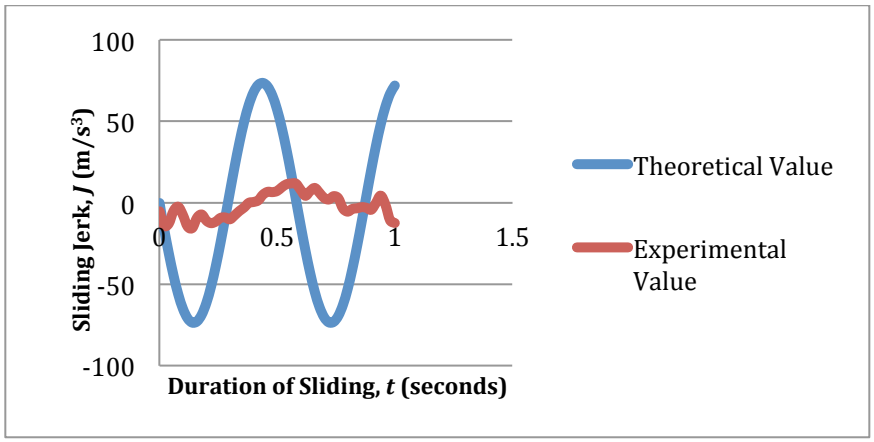

Figure 4.16- Effects of boundary friction on sliding jerk for both theoretical modeling and experimental studies when applied force is constant

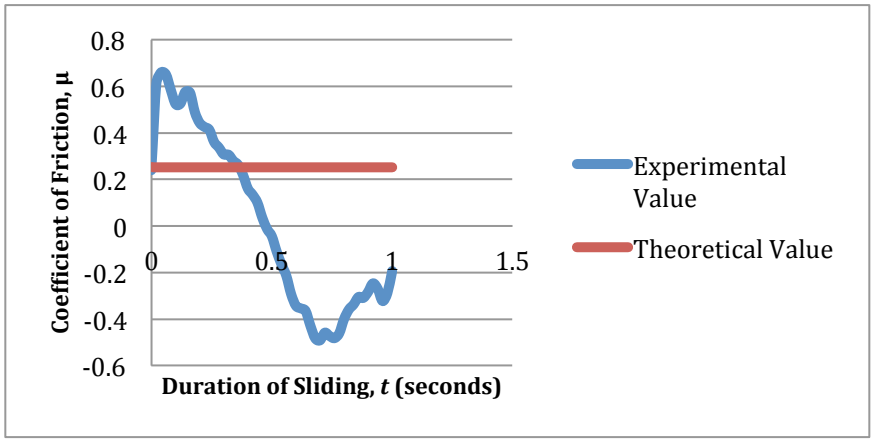

Figure 4.17- Effects of boundary friction on coefficient of friction for both theoretical modeling and experimental studies when applied force is constant

4.2.1.1 Discussion of results

1. From fig 4.13, it can be seen that experimental and theoretical instantaneous distances are almost similar till 0.5 second. The theoretical distance covered exceeds the experimental distance at the end of 0.5 seconds. But after 0.5 seconds, the theoretical distance reduces to zero before rising to a positive value. On the other hand, it can be seen that although the experimental instantaneous distance attempts to mimic the theoretical distance it could not follow the perfect sinusoid from theory as expected.
2. As can be seen from Fig. 4.14, the experimental instantaneous velocity are similar to the theoretical velocity although the latter has minimal fluctuations.
3. Fig. 4.15 shows how acceleration behaves instantaneously from both experimental results and the theoretical calculations. Although the experimental and theoretical results follow a similar trend, the maximum and minimum values do not match exactly.

4. It can be observed closely from Fig. 4.16 that the theoretical instantaneous jerk starts from zero and goes down to a negative value. Contrarily, the experimental jerk fluctuates within a minimal range while seeming to mimic the theoretical trend.

5. While the theoretical instantaneous friction coefficient is constant, it can clearly be seen from Fig. 4.22, how experimental instantaneous friction coefficient increases before going negative, capturing how the cart moves back when the friction force changed its direction.

6. The application of a constant force with a spring of required spring constant was not possible in the experiments. That is why we see deviations of experimental responses from theoretical modeling.

4.2.2 Subcase-2: Exponentially decreasing force with boundary friction

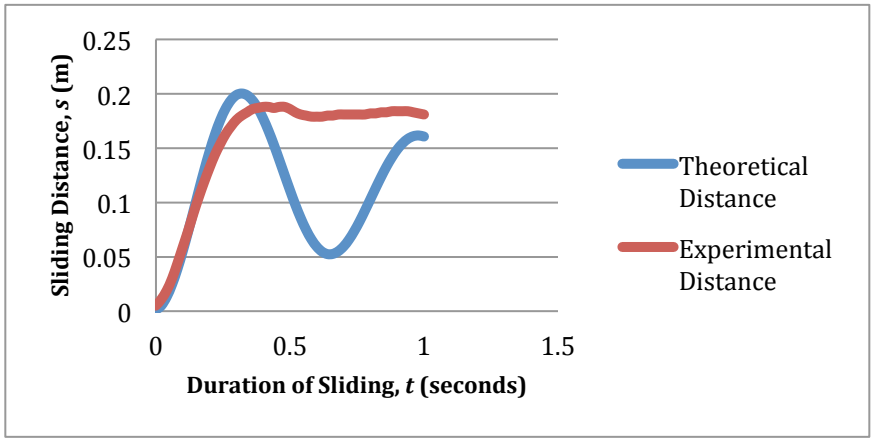

Figure 4.18- Effects of boundary friction on sliding distance for both theoretical modeling and experimental studies when applied force is decreasing exponentially

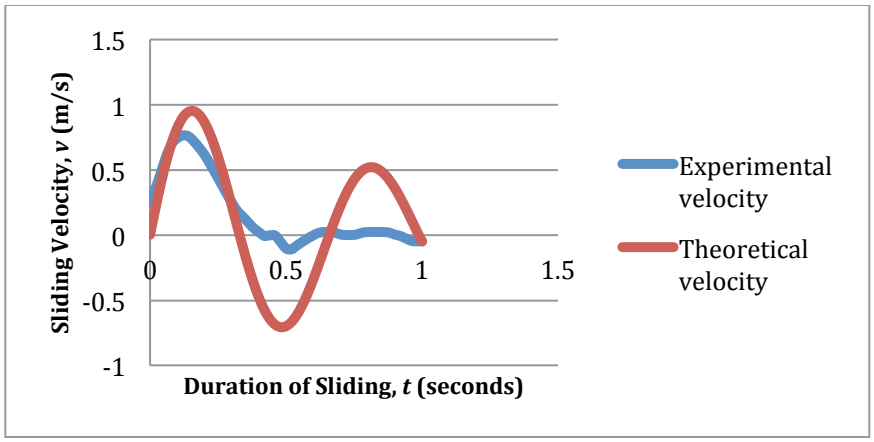

Figure 4.19- Effects of boundary friction on sliding velocity for both theoretical modeling and experimental studies when applied force is decreasing exponentially

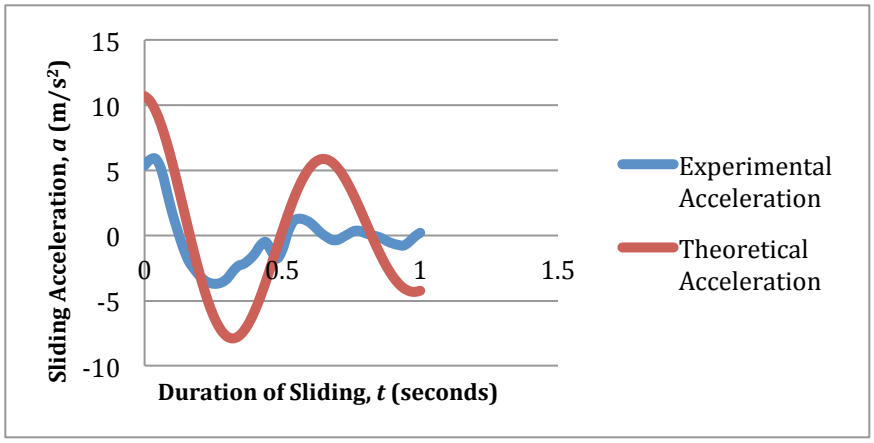

Figure 4.20- Effects of boundary friction on sliding acceleration for both theoretical modeling and experimental studies when applied force is decreasing exponentially

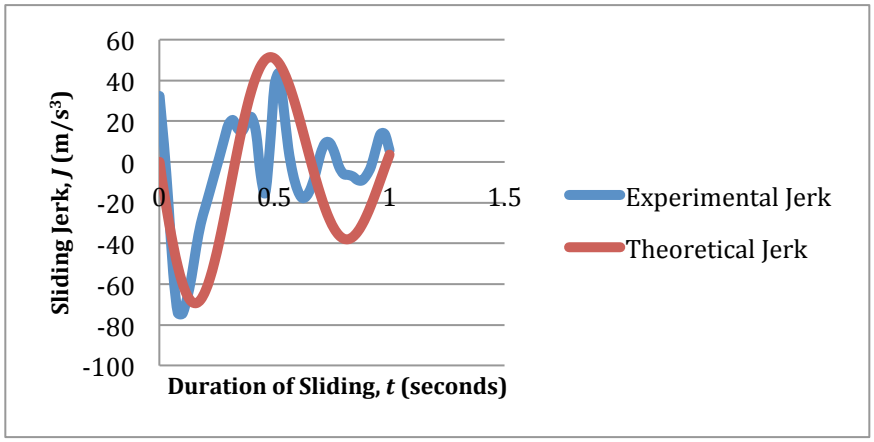

Figure 4.21- Effects of boundary friction on sliding jerk for both theoretical modeling and experimental studies when applied force is decreasing exponentially

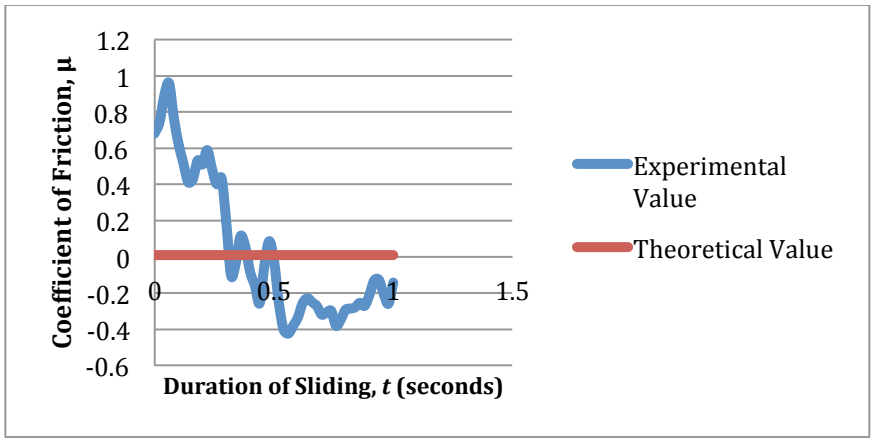

Figure 4.22- Effects of boundary friction on coefficient of friction for both theoretical modeling and experimental studies when applied force is decreasing exponentially

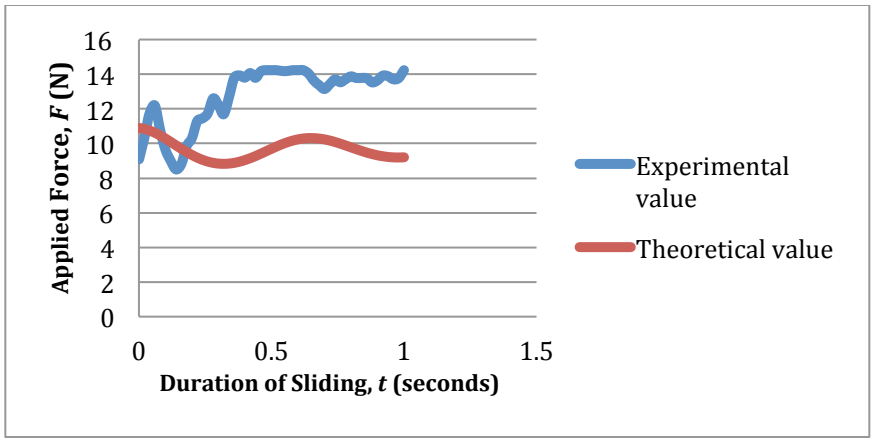

Figure 4.23- Effects of boundary friction on applied force for both theoretical modeling and experimental studies

4.2.2.1 Discussion of results

1. From Fig. 4.18 it can be seen that experimental and theoretical instantaneous distances are almost similar till 0.5 second. The theoretical distance subsequently exceeds the experimental distance at the end of 0.5 seconds. But after 0.5 seconds, the theoretical instantaneous distance decreases before increasing. On the other hand, it can be seen that although the experimental distance attempts to follow a similar trend, it becomes constant showing that the cart no longer moving.
2. As seen from Fig. 4.19, velocity follows the same trend as distance.
3. Figure 4.20 shows theoretical and experimental instantaneous accelerations. The experimental and theoretical accelerations begin similarly although after 0.5 seconds the experimental acceleration becomes negative (capturing deceleration) and moves close to zero as the cart stops as expected.
4. It can be observed closely from Fig. 4.21 that instantaneous theoretical jerk starts from zero and decreases to a negative value. Contrarily, the experimental instantaneous jerk becomes negative after beginning from a positive value. Also,

after 0.5 seconds the experimental jerk fluctuates more as the cart came to stop. There is still a noticeable similar trend.

5. While theoretical friction coefficient is constant, it can clearly be seen how experimental friction coefficient increases and again goes to negative value, showing how the cart moves backwards as the friction force changes its direction. However, theoretically, force is decreasing exponentially but in experiments it was hard to maintain application of force that way.
6. From figure 4.23 it can be seen that, the exponentially decaying force that was applied for the theoretical modeling could not be applied for experiments. That is why deviations are observed in the theoretical results.

Chapter 5

Conclusion, Comments, and Suggestions for Future Research

5.1 Comments and conclusions:

From the theoretical analyses and experimental results and the comparisons between the two, the following comments and conclusions were made:

1. From the results of theoretical modeling, while horizontal terminal motion is observed when constant force is applied but it is noticeably absent during the application of an exponentially decaying force.
2. It can also be seen from the theoretical modeling that there is an interesting coupling between drag and boundary friction effect (for example, the crossover points for acceleration, jerk, and mechanical efficiency) worth investigating further.
3. From the theoretical modeling and experimental results it can be observed that boundary friction adversely affects mechanical responses.
4. From the results of the experiments, it can be seen that none of the cases showed constant friction coefficient. While experimenting with spring-loaded sliding objects, friction coefficients dropped down to a negative value showing the cart was moving back as the friction force changed directions. It can be concluded that coefficient of friction can be negative when friction force changes direction, which also may signify an object's sliding interface encountering a lubricating effect.
5. Coefficient of friction increases during braking due to interfacial asperity.
6. While maintaining a constant force, the cart took very little time to cover a given distance but with an exponentially decreasing force applied, the cart took more time

to reach a similar distance. This is understandable because by reducing the available applied force through an exponential decrement, it is theoretically expected that given the same resistance, an object must use a longer time to cover a desired distance.

7. Without the resistance of a spring, acceleration seems to behave oppositely to the coefficient of friction. This evidence may align with Newton's second law of motion and requires further investigation.
8. While applying a constant force, the average instantaneous coefficient of friction was about 0.7 but when applying exponentially decreasing force, the coefficient of friction was noticeably smaller as low as 0.01. The reason for the decrease instantaneous coefficient of friction seems unclear and may require further investigation to understand the mechanisms at play.

5.2 Suggestions for future research

From the studies carried out in this thesis a few suggestions are proposed from improving the generality and relevance of the phenomena involving the resisted motion studied.

1. It is important to consider the modeling and experimental case studies that include interfacial boundary lubrication. This is important to understand how lubrication minimizes frictional dissipation, reduces wear and thereby improves mechanical efficiency.
2. In future modeling and experiments, it is also important to incorporate rough surfaces in sliding contacts to mimic actual operational conditions.

3. It will be instructive to create analytical solution techniques for verifying the numerical solutions of the nonlinear second order ordinary differential equations encountered.
4. In experimenting with the spring-loaded mass, viscous damping and aerodynamic drag must be included for a more complete theoretical picture.
5. The application of an exponentially decaying force should be kept same in experiments as in theoretical modeling. Devising an exponentially varying applied force for experimental purposes will be an invaluable research tool.

LIST OF REFERENCES

[1] S. Chu and A. Majumdar, Nature 488 (2012) 294.

[2] M. Urbakh, J. Klafter, D. Gourdon, and J. Israelachvili, Nature 430 (2004) 525.

[3] L. Binquan and O. R. Mark, Nature 435 (2005) 929.

[4] J. Williams, Engineering Tribology, Cambridge University Press, New York, 2005.

[5] N. P. Suh, Tribophysics, Prentice-Hall, Inc., New Jersey, 1986.

[6] G. W. Stachowiak and A. W. Batchelor, Engineering Tribology, Elsevier Inc., Burlington, MA, 2005.

[7] E. Rabinowicz, Friction and Wear of Materials, John Wiley & Sons, Inc., New York, 1995.

[8] K. Holmberg, R. Siilasto, T. Laitinen, P. Andersson, and A. Jäsberg, Tribology International 62 (2013) 58.

[9] K. Holmberg, P. Andersson, and A. Erdemir, Tribology International 47 (2012) 221.

[10] P. J. Blau, Tribology International 38 (2005) 1007.

[11] P. J. Blau, Journal of Materials Engineering 13 (1991) 47.

[12] B. Bhushan, Principles and Applications of Tribology, John Wiley & Sons, New York, NY, 1999.

[13] B. Armstrong-Hélouvry, P. Dupont, and C. C. De Wit, Automatica 30 (1994) 1083.

[14] B. Armstrong-Hélouvry, Control of Machines with Friction, Springer US, 1991.

[15] D. M. Bushnell, Viscous drag reduction in boundary layers, AIAA, 1990.

[16] W.-C. Yang, Industrial & Engineering Chemistry Fundamentals 12 (1973) 349.

[17] A. Kireenkov, S. Semendyaev, and V. Filatov, Mechanics of Solids 45 (2010) 921.

[18] P. D. Weidman and C. P. Malhotra, Physica D: Nonlinear Phenomena 233 (2007) 1.

[19] P. Weidman and C. P. Malhotra, Physical review letters 95 (2005) 264303.

[20] W.-H. Hucho, in Aerodynamics of Road Vehicles (W.-H. Hucho, ed.), Butterworth-Heinemann, 1987, p. 106.

[21] E. Aljallis, M. A. Sarshar, R. Datla, V. Sikka, A. Jones, and C.-H. Choi, Physics of Fluids 25 (2013) 025103.

[22] G. McHale, N. J. Shirtcliffe, C. R. Evans, and M. I. Newton, Applied Physics Letters 94 (2009) 064104.

[23] S. Gudmundsson, in General Aviation Aircraft Design (S. Gudmundsson, ed.), Butterworth-Heinemann, Boston, 2014, p. 661.

[24] R. K. Cooper, Journal of Wind Engineering and Industrial Aerodynamics 17 (1984) 215.

[25] S. Watkins, J. W. Saunders, and P. H. Hoffmann, Journal of Wind Engineering and Industrial Aerodynamics 57 (1995) 1.

[26] K. R. Cooper and W. F. Campbell, Journal of Wind Engineering and Industrial Aerodynamics 9 (1981) 167.

[27] S. J. Hands and M. M. Zdravkovich, Journal of Wind Engineering and Industrial Aerodynamics 9 (1981) 137.

[28] J. P. Howell, in Sustainable Vehicle Technologies (G. Warwickshire, ed.), Woodhead Publishing, 2012, p. 145.

[29] P. Wang and H. Pruppacher, Journal of Applied Meteorology 16 (1977) 275.

[30] M. Ohta, T. Imura, Y. Yoshida, and M. Sussman, International Journal of Multiphase Flow 31 (2005) 223.

[31] M. Wu and M. Gharib, Physics of Fluids (1994-present) 14 (2002) L49.

[32] G. P. Celata, F. D'Annibale, P. Di Marco, G. Memoli, and A. Tomiyama, Experimental thermal and fluid science 31 (2007) 609.

[33] M. Wegener, M. Kraume, and A. R. Paschedag, AIChE journal 56 (2010) 2.

[34] M. A. Talaia, World Academy of Science, Engineering and Technology 28 (2007) 264.

[35] H. J. Lamers, T. P. Snow, and D. M. Lindholm, The Astrophysical Journal 455 (1995) 269.

[36] D. C. Abbott, The Astrophysical Journal 225 (1978) 893.

[37] M. Coltelli, L. Miraglia, and S. Scollo, Bulletin of volcanology 70 (2008) 1103.

[38] E. Y. A. Wornyoh, C. F. Higgs, III, and R. Pudjoprawoto, ASME Conference Proceedings 2010 (2010) 449.

[39] E. Y. A. Wornyoh, in Mechanical Engineering, Vol. PhD, Carnegie Mellon University, Pittsburgh, 2009, p. 176.

[40] G. Di Toro, R. Han, T. Hirose, N. De Paola, S. Nielsen, K. Mizoguchi, F. Ferri, M. Cocco, and T. Shimamoto, Nature 471 (2011) 494.

[41] O. Ben-David, S. M. Rubinstein, and J. Fineberg, Nature 463 (2010) 76.

[42] E. Y. A. Wornyoh, D. K. Patel, L. D. Schuessler, A. B. Francis, and C. S. Garnett, in STLE/ASME International Joint Tribology Conference, Paper No. IJTC2011-61210, Los Angeles, CA, 2011.

[43] E. Y. A. Wornyoh, D. K. Patel, and L. D. Schuessler, in ASME/IMECE 2011 Paper No. IMECE2011-61614 Denver, CO, 2011.

[44] A. Socoliuc, E. Gnecco, S. Maier, O. Pfeiffer, A. Baratoff, R. Bennewitz, and E. Meyer, Science 313 (2006) 207.

[45] I. L. Singer, Journal of Vacuum Science & Technology a-Vacuum Surfaces and Films 12 (1994) 2605.

[46] A. Luedtke, Advanced Engineering Materials 6 (2004) 142.

[47] A. Wang, B. Edwards, S.-S. Yau, V. K. Polineni, A. Essner, R. Klein, D. C. Sun, C. Stark, and J. H. Dumbleton, in Proceedings of the 1996 Symposium on Characterization and Properties of Ultra-High Molecular Weight Polyethylene, November 19, 1996 - November 19, 1996, Vol. 1307, ASTM, New Orleans, LA, USA, 1998, p. 56.

[48] L. Que, L. D. T. Topoleski, and N. L. Parks, Journal of Biomedical Materials Research 53 (2000) 111.

[49] M. C. Galetz and U. Glatzel, Journal of the Mechanical Behavior of Biomedical Materials 3 (2010) 331.

[50] A. Abdelgaied, F. Liu, C. Brockett, L. Jennings, J. Fisher, and Z. M. Jin, Journal of Biomechanics 44 (2011) 1108.

[51] C. Putman and R. Kaneko, Thin Solid Films 273 (1996) 317.

[52] J. P. Gao, W. D. Luedtke, D. Gourdon, M. Ruths, J. N. Israelachvili, and U. Landman, Journal of Physical Chemistry B 108 (2004) 3410.

[53] B. Bushan, Principles and Applications of Tribology, John Wiley & Sons, Inc., New York, 1999.

[54] K.-H. Z. GAHR, Amsterdam: Elsevier, 1987.

[55] M. Tabor, Nature 310 (1984) 277.

[56] H. D. Young, R. A. Freedman, and A. L. Ford, 2007.

[57] I. M. Hutchings and P. Shipway, (1992)

[58] P. D. Weidman and C. P. Malhotra, Physical Review Letters 95 (2005) 264303.

[59] A. Khamooshi, T. Taylor, and D. W. Riggins, Aiaa Journal 45 (2007) 2401.

[60] E. Aljallis, M. A. Sarshar, R. Datla, V. Sikka, A. Jones, and C.-H. Choi, Physics of Fluids (1994-present) 25 (2013) 025103.

[61] M. A. Samaha, H. V. Tafreshi, and M. Gad-el-Hak, Colloids and Surfaces A: Physicochemical and Engineering Aspects 399 (2012) 62.

[62] M. Y. Corapcioglu, A. Cihan, and M. Drazenovic, Water resources research 40 (2004)

[63] A. Pytel and J. Kiusalaas, Engineering Mechanics: Dynamics, Cengage Learning, 2009.

[64] R. L. Norton, Design of Machinery: An Introduction to the Synthesis and Analysis of Mechanisms and Machines, McGraw-Hill Higher Education, 2008.

[65] H. Josephs and R. Huston, Dynamics of Mechanical Systems, CRC Press, 2002.

[66] M. F. Golnaraghi, Automatic control systems / Farid Golnaraghi, Benjamin C. Kuo, Hoboken, NJ : Wiley, c2010., Hoboken, NJ, 2010.

[67] M. Cieplak, E. D. Smith, and M. O. Robbins, Science 265 (1994) 1209.

[68] A. Akay, B. Echols, J. Q. Ding, A. Dussaud, and A. Lips, Wear 276 (2012) 61.

[69] R. W. Fox and A. T. McDonald, Introduction to fluid mechanics, John Wiley, 1994.

[70] J. A. Tichy and D. M. Meyer, International Journal of Solids and Structures 37 (2000) 391.

[71] H. Struchtrup and M. A. Rosen, Exergy, an International Journal 2 (2002) 152.

[72] I. I. Samkhan, Open Fuels & Energy Science Journal 2 (2009) 10.

[73] S. Radu, H. Abăităncei, A. Tuşinean, G.-A. Radu, and M. Iakab-Peter, in Proceedings of the European Automotive Congress EAEC-ESFA 2015, Springer, 2016, p. 641.

[74] L. B. Erbay and H. Yavuz, International journal of energy research 23 (1999) 863.

[75] N. Lutsey and D. Sperling, Transportation Research Record: Journal of the Transportation Research Board (2005) 8.

[76] E. Hellström, M. Ivarsson, J. Åslund, and L. Nielsen, Control Engineering Practice 17 (2009) 245.

[77] U. Hammarström, J. Eriksson, R. Karlsson, and M. R. Yahya, (2012)

[78] M. R. Cuddy and K. B. Wipke, SAE Technical Paper, 1997.

[79] A. Comfort, SAE Technical Paper, 2003.

[80] L. Cheah, C. Evans, A. Bandivadekar, and J. Heywood, in Reducing Climate Impacts in the Transportation Sector, Springer, 2008, p. 49.

[81] A. Cappiello, I. Chabini, E. K. Nam, A. Lue, and M. A. Zeid, in Intelligent Transportation Systems, 2002. Proceedings. The IEEE 5th International Conference on, IEEE, 2002, p. 801.